

# Evaluation of a Deposit in the Vicinity of the PBU L-106 Site, North Slope, Alaska, for a Potential Long-Term Test of Gas Production From Hydrates

G.J. Moridis, SPE; M.T. Reagan, SPE; K. Boyle, and K. Zhang, SPE, Lawrence Berkeley National Laboratory

## Abstract

As part of the effort to investigate the technical feasibility of gas production from hydrate deposits, a long-term field test (lasting 18-24 months) is under consideration in a project led by the U.S. Department of Energy. We evaluate a candidate deposit involving the C-Unit in the vicinity of the PBU-L106 site in North Slope, Alaska. This deposit is stratigraphically bounded by impermeable shale top and bottom boundaries (Class 3), and is characterized by high intrinsic permeabilities, high porosity, high hydrate saturation, and a hydrostatic pressure distribution. The C-unit deposit is composed of two hydrate-bearing strata separated by a 30-ft-thick shale interlayer, and its temperature across its boundaries ranges between 5 and 6.5 °C.

We investigate by means of numerical simulation involving very fine grids the production potential of these two deposits using both vertical and horizontal wells. We also explore the sensitivity of production to key parameters such as the hydrate saturation, the formation permeability, and the permeability of the bounding shale layers. Finally, we compare the production performance of the C-Unit at the PBU-L106 site to that of the D-Unit accumulation at the Mount Elbert site, a thinner, single-layer Class 3 deposit on the North Slope of Alaska that is shallower, less-pressurized and colder (2.3 – 2.6 °C). The results indicate that production from horizontal wells may be orders of magnitude larger than that from vertical ones. Additionally, production increases with the formation permeability, and with a decreasing permeability of the boundaries. The effect of the hydrate saturation on production is complex and depends on the time frame of production. Because of higher production, the PBU-L106 deposit appears to have an advantage as a candidate for the long-term test.

## Introduction

**Background.** Gas hydrates (GH) are solid crystalline compounds of water and gaseous substances described by the general chemical formula  $G \cdot N_H H_2O$ , in which the molecules of gas  $G$  (referred to as guests) occupy voids within the lattices of ice-like crystal structures. Hydrate deposits occur in two distinctly different geographic settings where the necessary conditions of low temperature  $T$  and high pressure  $P$  exist for their formation and stability: in the Arctic (typically in association with permafrost) and in deep ocean sediments (Kvenvolden, 1988).

The majority of naturally occurring hydrocarbon gas hydrates contain  $CH_4$  in overwhelming abundance. Simple  $CH_4$ -hydrates concentrate methane volumetrically by a factor of ~164 when compared to standard  $P$  and  $T$  conditions (STP). Natural  $CH_4$ -hydrates crystallize mostly in the structure I form, which has a hydration number  $N_H$  ranging from 5.77 to 7.4, with  $N_H = 6$  being the average hydration number and  $N_H = 5.75$  corresponding to complete hydration (Sloan and Koh, 2008). Natural GH can also contain other hydrocarbons (alkanes  $C_nH_{2n+2}$ ,  $n = 2$  to 4), but may also contain trace amounts of other gases (mainly  $CO_2$ ,  $H_2S$  or  $N_2$ ).

Although there has been no systematic effort to map and evaluate this resource on a global scale, and current estimates of in-place volumes vary widely (ranging between  $10^{15}$  to  $10^{18}$   $m^3$  at standard conditions), the consensus is that the worldwide quantity of hydrocarbon GH is vast (Milkov, 2004; Kluda and Sandler, 2005; Sloan and Koh, 2008). Given the sheer magnitude of the resource, ever increasing global energy demand, and the finite volume of conventional fossil fuel resources, GH are emerging as a potential energy source for a growing number of nations. The attractiveness of GH is further enhanced by the environmental desirability of natural gas, as it is an energy resource with a significantly lower carbon intensity than coal, oil, or other solid and liquid fuels. Thus, the appeal of GH accumulations as future hydrocarbon gas sources is rapidly increasing and their production potential clearly demands technical and economic evaluation. The past decade has seen a marked acceleration in gas hydrate R&D, including both a proliferation of basic scientific endeavors as well as the strong emergence of focused field studies of GH productivity, primarily within national GH programs (Moridis et al., 2009; 2010a). Together, these efforts have helped to clarify the dominant issues and challenges facing the extraction of methane from gas hydrates.

**Classification of Gas Hydrate Deposits and Production Methods.** Natural GH accumulations are divided into three main classes (Moridis and Collett, 2004) based on simple geologic features and the initial reservoir conditions. Class 1 settings are composed of two layers: a Hydrate-Bearing Layer (HBL) and an underlying two-phase fluid zone of mobile gas and liquid water. Because the base of the gas-hydrate stability zone (BGHSZ) coincides with the bottom of the HBL, this is the most desirable system as it is the easiest to destabilize and release gas (Moridis et al., 2008a; 2009). Class 2 settings comprise an HBL, overlying a zone of mobile water. Class 3 accumulations are composed of a single HBL, and are characterized by the absence of an underlying zone of mobile fluids. In Classes 2 and 3, the entire HBL may be at or well within the hydrate stability zone. A fourth class (Class 4) is typical of many oceanic accumulations, and involves dispersed, low-saturation hydrate (<10%) deposits that lack confining geologic strata and are not targets for production (Moridis and Sloan, 2007).

Gas can be produced from GH by inducing dissociation by one of the following main methods (Makogon, 1997): (1) depressurization, in which the pressure  $P$  is lowered to a level lower than the hydration pressure  $P_e$  at the prevailing temperature  $T$  – see Figure 1, (2) thermal stimulation, in which  $T$  is raised above the hydration temperature  $T_e$  at the prevailing  $P$ , and (3) the use of inhibitors (such as salts and alcohols), which shifts the  $P_e$ - $T_e$  equilibrium. Long-term production strategies often involve combinations of the three main dissociation methods (Moridis and Reagan, 2007a,b). Another production method involves  $\text{CH}_4$  exchange with another hydrate-forming gas (e.g.,  $\text{CO}_2$ ) through a thermodynamically favorable reaction (White and McGrail, 2008; Graue et al., 2008).

**Objectives.** This investigation is part of an effort led by the U.S. Department of Energy to identify appropriate targets for a long-term field test of production from permafrost-associated hydrate deposits (Boswell et al, 2008). The main objectives of this study are:

- (a) To evaluate the gas production potential of the C-Unit hydrate accumulation at the PBU L-106 site, North Slope, Alaska, during the planned long-term test
- (b) To determine through sensitivity analysis the conditions and properties that affect the production performance, and which can serve as criteria to identify other deposits as suitable candidate for a successful field test of production if the hydrate deposit at the PBU L-106 site is deemed unsatisfactory,
- (c) To determine the system response after the cessation of the long-term field test (i.e., after the well shut-in), and
- (d) To compare the production performance from the C-Unit hydrate accumulation at the PBU L-106 site to that from the D-Unit deposit at the Mount Elbert site, North Slope, Alaska, which was the subject of an earlier study (Moridis et al., 2010b)

### **The PBU-L106 Site, North Slope, Alaska**

**Regional Geological System Description.** The geology and petroleum geochemistry of the rocks on the North Slope of Alaska where gas hydrates are encountered are described in considerable detail in a number of publications (Bird and Magoon, 1987; Collett, 1993). The first direct confirmation of gas hydrate on the North Slope was provided by data from a single well (the Northwest Eileen State-2 well, located in the northwest part of the Prudhoe Bay Field), in which studies of pressurized core samples, downhole logs, and production testing had confirmed the occurrence of three gas-hydrate-bearing stratigraphic units (Collett, 1993).

Analysis of downhole log data from an additional 50 exploratory and production wells in the same area provided additional indications of hydrate occurrence in six laterally continuous sandstone and conglomerate units (A to F), which are all confined to the geographical area shown in Figures 2 and 3. Collett (2007) indicated that the hydrate units appear to trap down-dip several large free-gas accumulations (Figure 3; Units A through D). The volume of gas within the Eileen Gas Hydrate Accumulation (Collett, 2007) is estimated at about twice the volume of known conventional gas in the Prudhoe Bay Field (Collett, 1993), and ranges between  $1.0 \times 10^{12}$  and  $1.2 \times 10^{12} \text{ m}^3 \text{ STP}$  (Collett, 2007).

**Previous Studies.** Previous and current studies of gas production from hydrates in the North Slope of Alaska involve collaborations that are spearheaded by the BP Exploration (Alaska - BPXA), Inc., the U.S. Department of Energy, and the U.S. Geological Survey (USGS), and involve several other organizations. In 2003, the USGS initiated a study to develop seismic interpretive methods to identify and characterize GH accumulations in northern Alaska. This study dealt primarily with the analysis of a 3-D seismic data set from the area of the Milne Point Field as provided to the USGS by BP Exploration Alaska, Inc. (Figure 2). Detailed analysis and interpretation of available 3-D and 2-D seismic data sets, along with seismic modeling and correlation with specially processed downhole well log data, has led to the development of a viable method for identifying sub-permafrost GH prospects within the gas hydrate stability zone in the Milne Point area (Lee et al., 2010; Inks et al., 2010). This effort is supported by the Methane Hydrate Research and Development Act (enacted by the U.S. Congress in 2000 and renewed in 2005), and aims to determine the viability of the North Slope hydrates as an energy source (Mount Elbert Science Team, 2007) through investigations that will culminate with a long-term (1.5-2 years) field test of gas production (Boswell et al, 2008).

Analysis of geophysical surveys and well log data led the team to the installation of a well in 2007 at a previously undrilled, fault-bounded accumulation named the “Mount Elbert” prospect to acquire critical reservoir data needed to develop a longer-term production test program. The Mount Elbert-01 well was drilled to a depth of 915 m using chilled oil-based drilling fluid to avoid the inhibitor-induced dissociation caused by the salts and alcohols in conventional muds. A remarkable achievement was the recovery of significant lengths of core from the hydrate intervals, which were used for subsequent analyses of pore water geochemistry, microbiology, gas chemistry, petrophysical properties, and thermal and physical properties. After a battery of well log surveys was completed, a Schlumberger Modular Dynamic Testing (MDT) was conducted in two reservoir-quality sandy hydrate-bearing sections with high  $S_H$  (60% to 75%). Gas was produced from the gas hydrates in each of the tests. This study has yielded one of the most comprehensive datasets yet compiled on a naturally occurring gas hydrate geologic deposit (Collett, 2007).

Extensive discussions of the Mount Elbert geology and analyses of the various tests conducted at the site can be found in Boswell et al. (2010).

**The Unit C Hydrate Deposit at the PBU L-106 Site.** The gas production performance of both the C- and D-Units at the Mount Elbert site (see Figure 2) during the proposed long-term test has been previously investigated (Anderson et al., 2008, Moridis et al., 2010b). Because of the relatively low temperature of these deposits due to their proximity to the permafrost (which lowers the amount of sensible heat available to fuel the endothermic dissociation process), the low pressure in these relatively shallow formations (which limit the maximum pressure drop attainable during the depressurization-induced hydrate dissociation and the corresponding gas production rate), and the extreme sensitivity of gas production to the hydrate temperature (Moridis and Reagan, 2007a,b; Moridis et al., 2010b), production from Units C and D at the Mount Elbert site was generally low. As a potentially more appealing alternative, the Prudoe Bay Unit (PBU) L-106 well site “down-dip” from the Mount Elbert site (Figure 4) was investigated. The hydrate deposits at this site are deeper, more pressurized and warmer, and thus hold a promise of higher gas production.

Unit C extends from a depth of  $z = 678.5$  m (2226 ft) to  $z = 723.6$  m (2374 ft), and is composed of two hydrate-bearing strata: the deeper C1 and the shallower C2, 18.9 m (62 ft) and 17.1 m (56 ft) thick, respectively. These are that separated by a 9.2 m (30 ft) thick shale interlayer. This is a deposit bounded by impermeable shale top and bottom boundaries (Class 3), and is characterized by high intrinsic permeability ( $k = 1$ -5 Darcys), high porosity ( $\phi = 0.4$ ), high hydrate saturation ( $S_H = 0.75$ ), a hydrostatic pressure  $P$  distribution varying between  $P_T = 7.3$  and  $P_B = 7.7$  MPa across the unit boundaries, and a temperature  $T$  ranging between  $T_T = 5$  and  $T_B = 6.5$  °C across the unit boundaries. In the absence of any samples or field data, the properties of the C-Unit (and its boundaries) at the PBU L-106 site are assumed to be the same as those of the C-Unit of the Mount Elbert site (Anderson et al., 2008), as they both belong to the same formation. These properties, as well as initial conditions such as pressure, temperature and saturations (which were unavailable at the site and were obtained from nearby wells), are listed in Table 1.

For reference, the single HBL of the D-Unit at the Mount Elbert site was thinner (11.3 m), had a  $T$  ranging between  $T_T = 2.3$  °C and  $T_B = 2.6$  °C at the HBL top and bottom, respectively, and  $P$  at the HBL top was a low  $P_T = 6.4$  MPa (Moridis et al., 2010b). The temperature difference between the two units is very important: the study of Moridis et al. (2010b) has shown that a rise by 1 °C in the temperature of the D-Unit of the Mount Elbert deposit can lead to an eight-fold increase in the gas production rate.

## The Numerical Models and Simulation Approach

**The numerical simulation code.** We used the TOUGH+HYDRATE simulator (Moridis et al., 2008b; Zhang et al., 2008) to conduct the numerical studies in this paper. This code (hereafter referred to as T+H) can model all the known processes involved in the system response of natural CH<sub>4</sub>-hydrates in complex geologic media, including the flow of fluids and heat, the thermophysical properties of reservoir fluids, thermodynamic changes and phase behavior, and the non-isothermal chemical reaction of CH<sub>4</sub>-hydrate formation and/or dissociation, which can be described by either an equilibrium or a kinetic model (Kim et al., 1998; Clarke and Bishnoi, 2001; Moridis and Kowalsky, 2008). T+H is a compositional simulator, and its formulation accounts for heat and up to four mass components (i.e., H<sub>2</sub>O, CH<sub>4</sub>, CH<sub>4</sub>-hydrate, and water-soluble inhibitors such as salts or alcohols) that are partitioned among four possible phases: gas, aqueous liquid, ice, and hydrate. The T+H code can describe all the 15 possible thermodynamic states (phase combinations) of the CH<sub>4</sub>+H<sub>2</sub>O system and any combination of the three hydrate dissociation methods. It can handle the phase changes, state transitions, strong nonlinearities and steep solution surfaces that are typical of hydrate dissociation problems. Because of the very large computational requirements of this type of problem and the use of very large grids, we used the distributed-memory, massively parallel version of the code (Zhang et al., 2008) in the simulations discussed in this paper.

**System geometry.** The geologic system in this study corresponds to a location at the PBU L-106 site where the two HBLs (C1 and C2) and the shale interlayer have the thicknesses and dimensions discussed earlier. This is a complex variant of a Class 3 setting, in which the C2 and C1 HBLs are overlain and underlain, respectively) by nearly impermeable boundaries, i.e., shale strata. Based on experience gained in earlier studies (Moridis and Reagan, 2007a,b; Moridis et al., 2008a) and preliminary scoping calculations, the simulation domain was extended 30 m into the overburden and underburden of the system, a distance that was deemed sufficient to allow accurate heat exchange with the deposit during the production period. The shale interlayer between C1 and C2 was assumed to be permeable, with a realistic  $k = 5 \times 10^{-15}$  m<sup>2</sup> (= 5 mD) and  $\phi = 0.05$ .

We investigated the performance of both vertical and horizontal wells. The case of the vertical well, a single well was completed along the entire lengths of both the C1 and C2 HBLs. Because this is a long-term test and there is no information on outer boundaries, an infinite-acting system was assumed, and the outer radius of the cylindrical domain of the hydrate system was  $r_{max} = 2000$  m.

Because of the lack of flow between C1 and C2 (caused by the shale interlayer), the horizontal well study involved two wells, one placed at the top of each one of the C1 and C2 HBLs HBL to capitalize on gas buoyancy and accumulation at this location, in addition to minimizing water production. In this case, the Cartesian domain was assumed to be rectangle in  $(x,y)$  with a length of 1000 m and a side of  $L_y = 1772.5$  m. This corresponded to the same area as the domain in the cylindrical (single well) study, thus ensuring consistency by having the same surface area and hydrate volume in each simulation configuration. Both the vertical and the horizontal wells had a radius  $r_w = 0.1$  m.

**Domain discretization.** For maximum accuracy, very fine grids were used in the simulation of production from both the cylindrical and rectangular sections of the hydrate deposit. The cylindrical domain of the single vertical well problem was discretized into  $247 \times 192 = 47,424$  gridblocks in  $(r,z)$ , resulting in a system of 189,696 equations. Discretization along the radial direction was non-uniform, increasing logarithmically from  $r_w$  to  $r_{max}$ , with  $\Delta r_0 = 0.05$  m. Discretization along the  $z$ -axis was uniform (with  $\Delta z = 0.3$  m) within the HBLs, the shale interlayer, and the boundaries in the immediate vicinity of the HBLs, but non-uniform (with  $\Delta z$  increasing) near the top and bottom of the domain. The Cartesian well of the horizontal well problem was discretized into  $300 \times 192 = 57,600$  gridblocks in  $(r,z)$ . Assuming an equilibrium reaction of hydrate dissociation during this long-term production process (Kowalsky and Moridis, 2007), and accounting for the water salinity, the grid resulted in a system of 230,400 equations.

In the study of the performance of the horizontal well, we used only a single slice of unit thickness on the  $(x,z)$  plane, i.e., perpendicular to the horizontal well. Implicit in this approach is the assumption of uniformity along the well length  $L_w$ , i.e., along the  $y$ -axis. While this assumption may not be always valid in light of expected pressure variations along the length of the well, it is a good first-order approximation, it can be used to bound the expected solution through the choice of an appropriate range of well pressures in the studied slices, and it allows high-definition in the description of the system behavior without resulting in a prohibitively large grid. As in the case of production from a single vertical well in a cylindrical section of the hydrate deposit, the 2D domain in  $(x,z)$  was discretized into  $300 \times 192 = 57,600$  gridblocks, resulting in a system of 230,400 equations. The vertical discretization was the same as in the case of the cylindrical system. Discretization along  $x$ -axis was non-uniform, increasing logarithmically from  $x_0 = r_w$  to  $L_x$ , with  $\Delta x_0 = 0.05$  m.

Such a fine discretization is important (and possibly necessary) for accurate predictions when solid phases such as ice and hydrates are involved (Moridis et al., 2007). This high degree of refinement provided the level of detail needed to capture important processes near the wellbore and in the entire hydrate-bearing zone.

**System properties and well description.** As discussed earlier, the hydraulic and thermal properties of the various geological media (the HBL and the confining layers) in the C-Unit at the PBU L-106 site were assumed to be the same as in the C-Unit of Mount Elbert because of continuity of the same formation. These were obtained from data based on the first field test at the site (Anderson et al., 2008), and are listed in Table 1. We assumed that the initial hydrate and aqueous saturations ( $S_H$  and  $S_A$ , respectively) were uniformly distributed in the HBL, and that the overburden and underburden had both the same properties. The relative permeability relationships and the corresponding parameters were based on data obtained from history matching of the results of MDT test that had been conducted at the C-Unit at the Mount Elbert site (Anderson et al., 2008). The capillary pressure relationships and parameters were determined from the particle size analysis of porous media samples from C-Unit at the Mount Elbert site (White, 2008), and were consistent with the  $\phi$  and  $k$  of the C-Unit at the PBU L-106 site.

Based on earlier studies that confirmed the validity of the approach (Moridis and Reagan, 2007b;c), we approximated wellbore flow by Darcian flow through a pseudo-porous medium describing the interior of the well. This pseudo-medium had  $\phi = 1$ , a very high  $k = 10^{-9}$ - $10^{-8}$  m<sup>2</sup> (=1,000-10,000 Darcies), a capillary pressure  $P_c = 0$ , a relative permeability that was a linear function of the phase saturations in the wellbore, and a low (but nonzero) irreducible gas saturation  $S_{irG} = 0.005$  (necessary to allow the emergence of a free gas phase in the well).

**Initial and boundary conditions.** The low effective permeability of the HBLs, the large system dimensions, and the relatively short production period resulted in an infinite-acting system in the simulations. We determined the initial conditions in the reservoir by following the initialization process described by Moridis and Reagan (2007a;b). In both the cylindrical and the rectangular systems, the uppermost and lowermost gridblock layers (i.e., at the top of the overburden and at the bottom of the underburden in the simulated domains, where  $\Delta z = 0.001$  m) were treated as boundaries with constant conditions and properties. The temperatures at the upper and lower domain boundaries ( $T_U$  and  $T_L$ , respectively) were determined through a trial-and-error simulation process that resulted in the known  $T_P$  and  $T_B$  across the HBL. Note that the shales in the overburden and underburden were treated as impermeable (Table 1).

Knowing (a) the depth at the base of the HBL, and (b) assuming that the pressures in the subsurface follow the hydrostatic distribution—a hypothesis supported by earlier observations (Wright et al., 1999) in hydrate accumulations—we determined the pressure  $P_T$  (at  $z = 678.5$  m) using the P-, T- and salinity-adjusted water density (1005 kg/m<sup>3</sup> at atmospheric pressure). Then, using  $P_T$  and the boundary temperatures  $T_T$  and  $T_B$ , the hydrostatic gradient and representative thermal conductivity values were employed to determine the P- and T-profiles in the domains by means of a short simulation.

For reasons explained in detail by Moridis and Reagan (2007b), depressurization appears to be the most effective dissociation strategy, and a constant-pressure regime (involving a constant bottomhole pressure  $P_w$  at the well) is the most promising method of gas production from Class 3 hydrate deposits because of its simplicity, its technical and economic effectiveness, the fast response of hydrates to the rapidly propagating pressure wave, the near-incompressibility of water, and the large heat capacity of water. Because of the high initial hydrate saturation  $S_H$  in the HBL, the effective permeability  $k_{eff}$  is very low and constant-rate production is not feasible, while pure thermal stimulation is an unattractive option because of its limited effectiveness for reasons discussed in detail by Moridis and Reagan (2007a).

The numerical representation of a constant  $P_w$  involves treating the well as an internal boundary. In the case of a vertical well, this boundary is placed in the gridblock above the uppermost cell in the well. By imposing a constant  $P_w$ , a thermal conductivity  $k_\theta = 0$  W/m/K, and a realistic (though unimportant) constant temperature  $T_w$  at this internal boundary, the correct constant bottomhole- $P$  condition was applied to the well while avoiding any non-physical temperature distributions in the well itself (the large advective flows into the uppermost gridblock from its immediate neighbor eliminated any unrealistic heat transfer effects that could have resulted from an incorrect  $k_\theta$  and/or  $T_w$ ). In our study, the  $P_w = 3.0$  MPa exceeds the pressure at the quadruple point PQ, thus eliminating the possibility of ice formation and the corresponding potentially adverse effect on  $k_{eff}$ .

**Simulation process and outputs.** The maximum simulation period was 2 years, i.e., the maximum expected duration of the long-term field test. In the course of the simulation, the following conditions and parameters were monitored: Spatial distributions of  $P$ ,  $T$ , and gas and hydrate phase saturations ( $S_G$  and  $S_H$ ); Volumetric rates of  $CH_4$  released from dissociation and of  $CH_4$  production at the well ( $Q_R$  and  $Q_P$ , respectively); Cumulative volumes of  $CH_4$  released from dissociation, produced at the well, or remaining in the deposit as free gas ( $V_R$ ,  $V_P$  and  $V_F$ , respectively); Water mass production rate at the well ( $Q_W$ ) and cumulative mass of produced water ( $M_W$ ).

### Production Using a Vertical Well

**Gas production and water production.** Figure 6 shows the evolution of  $Q_R$  and  $Q_P$  from the single vertical well at the center of the cylindrical reservoir over time. The most important conclusions from the review of Figure 6 is that (a) the  $Q_R$  and  $Q_P$  increase monotonically, (b) they are very close in value, with  $Q_R$  being slightly higher than  $Q_P$ , and (c)  $Q_R$  and  $Q_P$  remain relatively low for the entire 2 years of the production period. Thus, at no time  $Q_R$  and  $Q_P$  exceed 2,500 ST m<sup>3</sup>/day (89,000 ST ft<sup>3</sup>/day) during the 2 years of the test. The low production rate is caused by the relatively low initial temperature of the hydrate in the HBLs. The low  $T$  reduces the rate of the dissociation reaction and severely reduces the sensible heat that is available to support it.

The cumulative produced volume  $V_P$  in Figure 7 provides further confirmation of the limited productivity of the C-Unit at the PBU L-106 site as a target for production from hydrates by depressurization using a vertical well: after continuous production for  $t = 2$  years,  $V_P < 8 \times 10^5$  ST m<sup>3</sup> ( $= 2.8 \times 10^7$  ST ft<sup>3</sup>) of  $CH_4$  have been produced.  $V_P < V_R$  during the entire production period (Figure 7). Note the very low level of free gas,  $V_F$ , in the reservoir during production (Figure 7), which exhibits a very mild upward trend during the 2 years of the test. The low levels of  $V_F$ , and the near-parity of  $V_R$  and  $V_P$  (and  $Q_R$  and  $Q_P$ ), indicate that there is little gas accumulation in the reservoir, and most of the gas released from dissociation and dissolution is produced at the vertical well.

The water production rate  $Q_W$  in Figure 8 reaches high level for a very short time at the beginning of production (when the pressure drop  $\Delta P = P_0 - P_w$  is at a maximum), then drops as the low  $k_{eff}$  of the HBLs does not allow large water flows, and then begins to increase continuously as the hydrate dissociates and  $k_{eff}$  increases. The most important observation from Figure 8 is that  $Q_W$  and  $M_W$  remain at easily manageable levels.

**Property distributions.** The evolution of  $P$ -distribution over time in Figure 9 is consistent with expectations. Pressure drops along the two production intervals, i.e., the entire thicknesses of the two HBLs. The permeable shale interlayer has initially higher permeability than the HBLs, resulting in a larger pressure drop there. As time advances, the area of depressurization increases. However, at  $t = 730$  days, it is easy to see from the last picture that only a fraction of the 2,000 reservoir radius is exhibiting depressurization, indicating that the system is indeed infinite-acting.

The evolution of  $T$ -distribution over time in Figure 10 shows a slowly (but consistently) expanding area of lower temperatures, denoting the expanding dissociation zone and the consequent cooling caused by the endothermic nature of the reaction. The evolutions  $S_H$  and  $S_G$  distributions in Figures 11 and 12, respectively, confirm the observations from Figures 6 and 7: hydrate dissociation appears to have barely affected the main body of the hydrate at the end of the 2-year production test, with signs of dissociation limited to a narrow zone around the production intervals and at the bounding planes of the 2 HBLs.

The low free gas volume  $V_F$  seen in Figure 7 is consistent with the observations from Figure 12, which shows very limited gas accumulation in the reservoir. Most of the gas is found along bottom of the C1 stratum and the top of the C2 layer, confirming the evolution of the upper dissociation interface that is the hallmark of all depressurization-induced dissociation behavior.

### Sensitivity Analysis

We investigated the sensitivity of gas production to the following conditions and parameters:

- (a) The initial hydrate saturation  $S_H$
- (b) The intrinsic permeability  $k$
- (c) The permeability of the shale boundaries  $k_B$
- (d) The type of the well (vertical vs. horizontal).

**Sensitivity to  $S_H$ .** Figure 13(a) shows that  $Q_R$  and  $Q_P$  increases with a decreasing  $S_H$ , at least within the range we investigated ( $0.50 \leq S_H \leq 0.75$ ). This is attributed to the higher  $k_{eff}$  that corresponds to lower  $S_H$  levels for a given intrinsic permeability  $k$ . However, the effect of  $S_H$  is a function of time. It can be seen that this behavior is not consistent: it holds true for times early in the production process, but it is completely reversed at later time. Thus, at  $t = 500$  days,  $Q_R$  and  $Q_P$  increases with an increasing  $S_H$ , but at  $t = 720$  days,  $Q_P$  for  $S_H = 0.50$  and  $S_H = 0.65$  are practically the same, and the trend is for  $Q_P$  for  $S_H = 0.50$  to be higher than that for  $S_H = 0.65$ . It is not known if this will be a persistent behavior or the result of temporary fluctuations. Note that the gap between  $Q_R$  and  $Q_P$  (with  $Q_R < Q_P$ ) increases with a decreasing  $S_H$ , indicating an increasing contribution of dissolved gas to total production; for  $S_H = 0.75$ ,  $Q_P < Q_R$ .

The evolution of the cumulative volumes  $V_R$  and  $V_P$  in Figure 13(b) reflects the relative sizes of  $Q_R$  and  $Q_P$ . Thus,  $V_R$  and  $V_P$  initially increase with a decreasing  $S_H$ , but the trend is reversed at later times. The levels of  $V_F$  are very low, indicating limited gas accumulation in the reservoir.

In Figure 14, the water production rates  $Q_w$  and cumulative mass of produced water  $M_w$  associated with depressurization-induced gas production from the hydrates at the PBU L-106 site show a clear pattern, increasing with a decreasing  $S_H$ . They differ very substantially for the various  $S_H$  in the study because they reflect drastically different  $k_{eff}$  regimes (strongly influenced by  $S_H$ ).  $Q_w$  decreases over time because the driving force  $\Delta P$  in the reservoir decreases as depressurization advances, and eventually the three  $Q_w$  appear to stabilize (at least within the time frame of this study – it is unlikely that this pattern will persist at later times).

**Sensitivity to the formation intrinsic permeability  $k$ .** Figure 15 shows that  $V_R$  and  $V_P$  both increase with an increasing  $k$ , (as do the corresponding  $Q_R$  and  $Q_P$ ). This was expected because a higher  $k$  leads to a higher  $k_{eff}$ . Similarly, the water production rates  $Q_w$  and the cumulative mass of produced water  $M_w$  in Figure 16 increase with an increasing  $k$ , and follow the same pattern identified in the reference case of Figure 8.

**Sensitivity to the intrinsic permeability of the shale boundaries  $k_B$ .** Figure 17 shows that both  $Q_R$  and  $Q_P$  decrease rapidly with an increasing  $k_B$  because of the reduced effectiveness of depressurization (as the permeable boundaries admit fluids and do not allow a sufficiently strong pressure drop). An increasing  $k_B$  leads to an imbalance in the magnitudes of  $Q_R$  and  $Q_P$ . From rough parity for  $k_B = 0$ ,  $Q_P$  becomes larger than  $Q_R$ , with increasing amounts of gas contributed from dissolved gas. Additionally, because of the increased permeability of the boundary, water production increases drastically (Figure 18).

## Production Using a Horizontal Well

**Gas production.** Figure 19 shows the evolution of  $Q_R$  and  $Q_P$  from a horizontal well over time, and includes for reference the  $Q_R$  and  $Q_P$  corresponding to the vertical well (from Figure 6). The use of the horizontal well is shown to increase both  $Q_R$  and  $Q_P$  by a minimum of a factor of 4 (and by well over an order of magnitude early in the production period). While the improvement in performance over the vertical well is dramatic,  $Q_P$  remains moderate in absolute terms. However, it is possible that the production outlook may improve with longer wells, different well configurations, more complex production strategies, and by the consideration of heterogeneity (which has been shown to improve production in layered systems such as the ones in Units C and D of Mount Elbert – see Kurihara et al., 2005; 2009).

The evolution of  $Q_R$  and  $Q_P$  is characterized by an initial period (Stage 1, to  $t = 300$  days) of linear increase, and is succeeded by a period of relative stability (stage 2) that lasts until the end of the long-term test at  $t = 720$  days. At the end of Stage 1,  $Q_P = 9 \times 10^3$  ST m<sup>3</sup>/day ( $= 3.2 \times 10^5$  ST ft<sup>3</sup>/day), and in Stage 2 it stabilizes at this level.

Stage 1 is associated with rapid depressurization (especially near the wellbore) and corresponds to the rapid advancement of the depressurization front in the deposit. Because (a) the pressure drop  $\Delta P = P_o - P_w$  between the bottomhole pressure and the pressure at the dissociation front is at its maximum  $\Delta P_{max}$  in the HBL, and (b) dissociation expands continuously into unaffected parts of the HBL as the depressurization front advances quickly,  $Q_R$  and  $Q_P$  increase rapidly and  $dQ_R/dt$  and  $dQ_P/dt$  are at their maximum. The endothermic nature of the hydrate dissociation reaction results in cooling of the HBL, but this has a limited effect in countering the effects of  $\Delta P$  on subsequent dissociation.

The end of Stage 1 and onset of Stage 2 is marked by the depressurization front reaching the outer boundaries of the HBL domain (i.e., at  $y = L_y$ ,  $x = L_x$ ). When this happens, the pressure wave can no longer advance, and the pressure drop at any point in the domain  $\Delta P = P - P_w < \Delta P_{max}$ . While  $Q_R$  and  $Q_P$  continue to increase because a larger volume of hydrate is dissociating, they do so slower, i.e., the lower pressure gradient leads to the reduction in  $dQ_R/dt$  and  $dQ_P/dt$ , which remain positive. Additionally, continuing HBL cooling caused by advancing hydrate dissociation makes further dissociation progressively more difficult.

Finally, the continuously diminishing driving force of dissociation (i.e., the  $\Delta P$ ) and the parallel reduction in the sensible heat that fuels and supports it eventually lead to a decline  $Q_R$  and  $Q_P$ . However, we do not observe it in our study because of the relatively short duration of the test and the low  $Q_R$  and  $Q_P$ , which do not materially affect the bulk of the hydrate mass in the 2-year time frame.

$Q_R$  and  $Q_P$  in Figure 19(a) are very similar in magnitude, as was the case in production from a vertical well. Similar to the reference case of the vertical well problem,  $Q_R > Q_P$  during production from the horizontal well. We observe a similar pattern in the relationship of  $V_R$  and  $V_P$  in Figure 19(b), with  $V_R$  being very slightly larger than  $V_P$ , while both (and  $V_F$ ) are several

times larger than the ones corresponding to the vertical well case. Review of the relative magnitudes of  $Q_R$ ,  $Q_P$ ,  $V_R$ ,  $V_P$ , and  $V_F$  confirms the pattern identified in the vertical well case, i.e., little gas accumulation in the reservoir, with most of the gas released from dissociation and dissolution is produced at the horizontal well. The cumulative produced volume  $V_P$  in Figure 19(b) provides further confirmation of the improved outlook, which, while not being spectacular, is respectable for onshore production.

**Water production.** The water production rate  $Q_W$  in Figure 20 exhibits fluctuations, but, after an initial phase of declining  $Q_W$ , appears on average to be roughly stable as it oscillates about a relatively stable mean. This is confirmed by the near-linear pattern of the  $M_W$  graph in Figure 20. A declining long-term trend is (a) an inevitable consequence of a continuously declining pressure differential  $\Delta P$ , and (b) consistent with observations and conclusions from previous studies of production from hydrates (Moridis et al, 2007a;b; Moridis et al., 2010b), but the short duration of the test and the small fraction of the hydrate mass that has been destroyed during it do not allow us to observe this decline. While  $M_W$  is larger (as expected) in the horizontal well case, it remains at manageable levels.

### System Response During A Well Shut-In

An important question that needs to be answered as the long-term field is planned is the response of the hydrate deposit upon the cessation of production because this will define the time frame of the study, and will address persistent worries that continuing dissociation after the well shut-in may cause complications. Figure 21 shows the evolution of  $Q_R$  (describing the net rate of hydrate dissociation in the entire deposit after a well shut in. The rates of  $\text{CH}_4$  release  $Q_R$  decrease initially.  $Q_R$  is initially positive (indicating continuing dissociation because of pressure gradients in the deposit after the well shut-in), but then becomes negative (indicating hydrate formation near the well as  $P$  increases). After a short time (the duration of which is closely related to the exhaustion of free gas in the deposit),  $Q_R$  drops rapidly to near-zero levels, indicating disappearance of free gas and cessation of hydrate formation or dissociation at  $t = 80 - 110$  days past the well shut in. Past that point, some low-level activity (indicated by  $Q_R > 0$ ) continues for a long time, and denotes long-term hydrate dissolution and redistribution as heat from the boundaries continues to flow into the deposit and a pressure and geothermal equilibrium are re-established.

The cumulative volume of released  $\text{CH}_4$  ( $V_R$ ) after the well shut-in in Figure 22 is positive in all cases, indicating continuing net hydrate dissociation. This is caused by residual pressure gradients that persist within the deposit, and which allow continuing dissociation away from the well. These pressure differentials decline rapidly, leading to higher pressures in the vicinity of the well (where  $T$  is low), secondary hydrate formation and rapidly declining  $V_R$ . This results in the negative  $V_R$  values that are observed after a short time (<10 days) following the well shut-in, which denote hydrate formation.

### Comparison to the Production Performance of Unit D at the Mount Elbert Site, North Slope, Alaska

Figure 23 shows the production and release rates  $Q_R$  and  $Q_P$  for the D-Unit at the Mount Elbert site (Moridis et al., 2010b) using both horizontal and vertical wells. If the magnitude of the rate of gas production is the absolute criterion for success of the proposed field test, then the superiority of the C-Unit at the PBU L-106 site is evident: the corresponding  $Q_R$  in Figure 19 is several times higher than that for the D-Unit at the Mount Elbert site. There are two reasons for this superior production performance. The first is the higher formation temperature, which is known to be probably the most important factor affecting production (all other issues being equal). The second reason is the considerably larger thickness of the HBLs at the PBU L-106 site, resulting in a larger gas source.

### Summary and Conclusions

This study is part of an effort led by the U.S. Department of Energy to identify appropriate targets for a long-term field test of production from permafrost-associated hydrate deposits. We focus on the evaluation of the gas production potential of a gas hydrate deposit in the C-Unit of the PBU L-106 site on the North Slope, Alaska. We investigate the performance of vertical and horizontal wells operating under constant bottomhole pressure in gas production fueled by depressurization-induced dissociation of the hydrates. Based on the results of this study, we draw the following conclusions:

- (1) Preliminary calculations indicate that a long-term test of gas production from a gas hydrate deposit (Unit C) at the PBU-L106 site using a single vertical well is feasible. The production rate  $Q_P$  is predicted to increase consistently during the duration of the long-term test (up to 2 years). However,  $Q_P$  is generally low because of relatively low temperatures (5 to 6.5 °C) and pressure (limiting the magnitude and effectiveness of depressurization), with a maximum  $Q_P = 2,250$  ST  $\text{m}^3/\text{day}$  (about 80 MSCFPD), and a cumulative volume of produced gas  $V_P = 80,000$  ST  $\text{m}^3$  (about 2.81 MMSCF).
- (2) The water production rates  $Q_W$ , and the corresponding cumulative mass of produced water  $Q_W$ , are modest and can be easily handled during production.
- (3)  $Q_W$  and  $M_W$  increase with an increasing intrinsic permeability  $k$ , and with a decreasing permeability of the shale boundaries (overburden and underburden)  $k_B$  of the hydrate deposit.

- (4) The effect of the initial hydrate saturation  $S_{H0}$  on  $Q_P$  and  $V_P$  is not monotonic or straightforward, and is a function of time; initially,  $Q_P$  and  $V_P$  increase with a decreasing  $S_{H0}$  because of a higher effective permeability (and, thus, easier dissociation), but the effect is reversed at later times.
- (5) The use of horizontal wells can increase  $Q_P$  and  $V_P$  by orders of magnitude (with a  $V_P$  reaching  $5.27 \times 10^6$  ST m<sup>3</sup> = 186 MMSCF at the end of the production test for a well of length  $L = 1000$  m). The corresponding increase in water production remains well within manageable limits.

### Acknowledgment

This work was supported by the Assistant Secretary for Fossil Energy, Office of Natural Gas and Petroleum Technology, through the National Energy Technology Laboratory, under the U.S. Department of Energy, Contract No. DE-AC02-05CH11231. The authors are indebted to John Apps and Dan Hawkes for their careful review.

### References

- Anderson, B.J., Wilder, J.W., Kurihara, M., White, M.D., Moridis, G.J., Wilson, S.J., Pooladi-Darvish, M., Masuda, Y., Collett, T.S., Hunter, R.B., Narita, H., Rose, K. and Boswell, R., 2008. Analysis of Modular Dynamic Formation Test Results From the Mount Elbert-01 Stratigraphic Test Well, Milne Point Unit, North Slope, Alaska, paper presented at the 6<sup>th</sup> International Conference on Gas Hydrates, Vancouver, British Columbia, Canada, July 6-10, 2008.
- Bird, K.J., and Magoon, L.B., 1987, Petroleum geology of the northern part of the Arctic National Wildlife Refuge, Northeastern Alaska: *U.S. Geological Survey Bulletin* **1778**, 324.
- Boswell, R., Hunter, R., Collett, T.S., Digert, S., Hancock, M., Weeks, M. 2008. Investigation of gas hydrate bearing sandstone reservoir at the Mount Elbert stratigraphic test well, Milne Point, Alaska. *Proc. 6th International Conference on Gas Hydrates*, July 6 – 10, 2008, Vancouver, BC.
- Boswell, R., Collett, T., Anderson, B., Hunter, R., eds., 2010, Scientific results of the BPXA-USDOE-USGS Mount Elbert gas hydrate stratigraphic test well, Milne Point Unit, Alaska North Slope. *J. Marine Pet. Geo.*
- Clarke, M.A., and Bishnoi, P.R., 2000. Determination of the Intrinsic Rate of Methane Gas Hydrate Decomposition”, *Chem. Eng. Sci.*, **55**, 4869.
- Collett, T., 1993, Natural gas hydrates of the Prudhoe Bay and Kuparuk River area, North Slope, Alaska: American Association of Petroleum Geologists Bulletin, **77** (5), 793-812.
- Collett, T., 1995. *1995 National Assessment of U.S. Oil and Gas Resources* (on CD-ROM) (Gautier, D.L., Goldton, G.L. et al., eds.), USGS.
- Collett, T., 2007. Arctic Gas Hydrate Energy Assessment Studies, The Arctic Energy Summit, ANCHORAGE, ALASKA • 15-18 OCTOBER 2007
- Dallimore, S.R., Uchida, T., and Collett, T.S., 1999, Scientific results from JAPEX/JNOC/GSC Mallik 2L-38 gas hydrate research well, Mackenzie Delta, Northwest Territories, Canada, *Geological Survey of Canada Bulletin* **544**, 403.
- Dallimore, S.R., and Collett, T.S., Eds., 2005. Scientific Results from the Mallik 2002 Gas Hydrate Production Research Well Program, Mackenzie Delta, Northwest Territories, Canada, *Geological Survey of Canada Bulletin* **585**.
- Graue, S., Kvamme, B., Baldwin, B.A., Stevens, J., Howard, J., Aspenes, E., Ersland, G., Husebo, J., Zomes, D., M. 2008. MRI Visualization of Spontaneous Methane Production From Hydrates in Sandstone Core Plugs When Exposed to CO<sub>2</sub>. *SPE J.* **13**(2): 146-152, (doi: 10.2118/118851-PA).
- Inks, T.L., Lee, M.W., Agena, W.F., Taylor, D.J., Collett, T.S., Hunter, R.B., Zyrianova, M.V., 2010. Seismic prospecting for gas hydrate and associated free-gas prospects in the Milne Point area of northern Alaska, in Collett, T., Johnson, A., Knapp, C., Boswell, R., eds, Natural Gas Hydrates -- Energy Resource Potential and Associated Geologic Hazards: *American Association of Petroleum Geologists Memoir* **89**.
- Kim, H.C., Bishnoi, P.R., Heidemann, R.A., and Rizvi, S.S.H., 1987. Kinetics of Methane Hydrate Decomposition, *Chem. Eng. Sci.*, **42**(7), 1645.
- Klauda, J.B., and Sandler, S.I., 2005. Global distribution of methane hydrate in ocean sediment, *Energy & Fuels* **19**, 469.
- Kowalsky, M. B., and Moridis, G.J., 2007, Comparison of kinetic and equilibrium reactions in simulating the behavior of gas hydrates, *Energy Conversion and Management*, **48**, 1850, doi:10.1016/j.enconman.2007.01.017 (LBNL-63357).
- Kurihara, M., Funatsu, K., Ouchi, H., Masuda Y. and Narita, H., 2005b. Investigation On Applicability Of Methane Hydrate Production Methods To Reservoirs With Diverse Characteristics, Paper 3003 presented at the 5th International Conference on Gas Hydrates, Trondheim, Norway, 13–16 June, Proceedings, Vol. 3, 714-725.
- Kurihara, M., Sato, A., Ouchi, H., Narita, H., Masuda, Y., Saeki, T., and Fujii, T. 2009. Prediction of Gas Productivity from Eastern Nankai Trough Methane-Hydrate Reservoirs. *SPE Res Eval & Eng* **12** (3): 477-499. SPE-125481-PA. doi: 10.2118/125481-PA.
- Kvenvolden, K.A., 1988. Methane hydrate--A major reservoir of carbon in the shallow geosphere? *Chem. Geo.* **71**: 41-51.
- Lee, M.W., Collett, T.S., Inks, T.L., 2010. Seismic attribute analysis for gas-hydrate and free-gas prospects on the North Slope of Alaska, in Collett, T., Johnson, A., Knapp, C., Boswell, R., eds, Natural Gas Hydrates -- Energy Resource Potential and Associated Geologic Hazards: *American Association of Petroleum Geologists Memoir* **89**.
- Milkov, A. V., 2004. Global estimates of hydrate-bound gas in marine sediments: How much is really out there? *Earth Science Reviews* **66** (3), 183.
- Makogon, Y.F., 1987. Gas hydrates: frozen energy, *Recherche* **18** (192), 1192.
- Makogon, Y.F., 1997. *Hydrates of Hydrocarbons*. Penn Well Publishing Co. Tulsa, OK.
- Moridis, G.J., 2003. Numerical Studies of Gas Production From Methane Hydrates, *SPE Journal*, **32**(8), 359.
- Moridis, G.J., Collett, T.S. 2004. Strategies for Gas Production from Hydrate Accumulations Under Various Geologic Conditions, LBNL-52568, Lawrence Berkeley National Laboratory, Berkeley, CA.

- Moridis, G.J., and Sloan, E.D., 2007. Gas Production Potential of Disperse Low-Saturation Hydrate Accumulations in Oceanic Sediments, *J. Energy Conversion and Management*, **48** (6), 1834-1849.
- Moridis, G.J., Collett, T., Dallimore, S., Satoh, T., Hancock, S., and Weatherhill, B., 2004. Numerical Studies Of Gas Production From Several Methane Hydrate Zones At The Mallik Site, Mackenzie Delta, Canada, *JPSE* **43**, 219.
- Moridis, G.J., and Reagan, M.T., 2007a. Strategies for Gas Production From Oceanic Class 3 Hydrate Accumulations, *OTC-18865*, 2007 Offshore Technology Conference, Houston, Texas, 30 April – 3 May 2007.
- Moridis, G.J., and Reagan, M.T., 2007b. Gas Production From Oceanic Class 2 Hydrate Accumulations, *OTC 18866*, 2007 Offshore Technology Conference, Houston, Texas, U.S.A., 30 April–3 May 2007.
- Moridis, G.J., and Reagan, M.T., 2007c. Gas Production From Class 2 Hydrate Accumulations in the Permafrost, *SPE 110858*, 2007 SPE Annual Technical Conference and Exhibition, Anaheim, California, U.S.A., 11–14 November 2007.
- Moridis, G.J., Sloan, E.D. 2007. Gas Production of disperse low-saturation hydrate accumulations in oceanic sediments. *Energy Conversion and Management* **48**: 1834-1849.
- Moridis, G.J., Kowalsky, M., and Pruess, K., 2008a. Depressurization-Induced Gas Production From Class 1 Hydrate Deposits, *SPE Reservoir Evaluation and Engineering*, **10** (5), 458-488.
- Moridis, G.J., Kowalsky, M.B., and Pruess, K., 2008b. TOUGH+HYDRATE v1.0 User's Manual: A Code for the Simulation of System Behavior in Hydrate-Bearing Geologic Media, Report LBNL-00149E, Lawrence Berkeley National Laboratory, Berkeley, CA.
- Moridis, G.J., Collett, T.S., Boswell, R., Kurihara, M., Reagan, M.T., Sloan, E.D., Koh, C., 2009. Toward production from gas hydrates: assessment of resources and technology and the role of numerical simulation. *SPE Reservoir Evaluation & Engineering*, 12(5): 745-771 (doi: 10.2118/114163-PA).
- Moridis, G.J., T.S. Collett, M. Pooladi-Darvish, S. Hancock, C. Santamarina, R. Boswell, T. Kneafsey, J. Rutqvist, M. Kowalsky, M.T. Reagan, E.D. Sloan, A.K. Sum and C. Koh, 2010a. Challenges, Uncertainties and Issues Facing Gas Production From Hydrate Deposits in Geologic Systems, Invited Paper SPE 131792, 2010 Unconventional Gas Conference, February 23-25, Pittsburgh, PA.
- Moridis, G.J., S. Silpngarmert, M.T. Reagan, T.S. Collett, and K. Zhang, 2010b. Gas Production From a Cold, Stratigraphically Bounded Hydrate Deposit at the Mount Elbert Site, North Slope, Alaska, In press, *Journal of Marine and Petroleum Geology*, 2010 (doi: 10.1016/j.marpetgeo.2010.01.005, LBNL-3005E).
- Reagan, M.T., Moridis, G.J., and Zhang, K., 2008. Sensitivity Analysis of Gas Production from Class 2 and Class 3 Hydrate Deposits, OTC 19554, 2008 Offshore Technology Conference, Houston, Texas, USA, 5-8 May 2008.
- Sloan, E.D., and Koh, C., 2008. *Clathrate Hydrates of Neutral Gases*. 3rd Edition, Taylor and Francis, Inc., Boca Raton, FL.
- Sun, X., and Mohanty, K.K., 2005. Simulation of Methane Hydrate Reservoirs, SPE 93015, 2005 SPE Reservoir Simulation Symposium, Houston, TX U.S.A., 31 January - 2 February 2005.
- van Genuchten, M.Th., 1980. A Closed-Form Equation for Predicting the Hydraulic Conductivity of Unsaturated Soils”, *Soil Sci. Soc.*, **44**, 892.
- White, M., 2008. Personal communication.
- White, M., McGrail, B.P, 2008. Numerical Simulation of Methane Hydrate Production from Geologic Formations via Carbon Dioxide Injection, Paper OTC-19458-MS, Offshore Technology Conference, 5-8 May 2008, Houston, Texas, USA (doi: 10.4043/19458-MS).
- Wright, J.F., Dallimore, S.R., and Nixon, F.M., 1999. Influences of Grain Size and Salinity on Pressure-Temperature Thresholds for Methane Hydrate Stability in JAPEX/JNOC/GSC Mallik 2L-38 Gas Hydrate Research-Well Sediments, in Scientific Results from JAPEX/JNOC/GSC Mallik 2L-38 Gas Hydrate Research-Well, Mackenzie Delta, Northwest Territories, Canada. Dallimore, S.R., Uchida, T., and Collett, T.S., Eds., *Geological Survey of Canada Bulletin* **544**, 229.
- Zhang, K., and Moridis, G.J., 2008. A Domain Decomposition Approach for Large-Scale Simulations of Coupled Processes in Hydrate-Bearing Geologic Media, paper presented at the 6<sup>th</sup> International Conference on Gas Hydrates, Vancouver, British Columbia, Canada, July 6-10, 2008.

<b>Table 1 – Hydrate Deposit Properties used in the study of Unit C, PBU L-106 (Taken from the C-Unit of Mount Elbert and nearby wells)</b>	
<b>Parameter</b>	<b>Value</b>
C1 Hydrate zone thickness	18.9 m
C2 Hydrate zone thickness	17.1 m
Shale interlayer tickness	9.2 m
Initial pressure at top of HBL ( $P_T$ )	7.3 MPa
Initial temperature at top of HBL ( $T_T$ )	5.0 °C
Initial temperature at base of HBL ( $T_B$ )	6.3 °C
Gas composition	100% CH <sub>4</sub>
Initial saturations in the HBL	$S_H = 0.75$ , $S_A = 0.25$
Intrinsic permeability of HBL $k_r = k_x = k_z$	$10^{-12}$ m <sup>2</sup> (= 1 D)
Porosity of HBL $\phi$	0.4
Compressibility of HBL	$5 \times 10^{-9}$ Pa <sup>-1</sup>
Intrinsic permeability $k_r = k_x = k_z$ (overburden & underburden)	0 m <sup>2</sup> (= 0 D)
Porosity of overburden & underburden	0.005
Grain density $\rho_R$ (all formations)	2750 kg/m <sup>3</sup>
Constant bottomhole pressure ( $P_w$ )	3 MPa
Dry thermal conductivity ( $k_{\theta RD}$ ) (all formations)	0.5 W/m/K
Wet thermal conductivity ( $k_{\theta RW}$ ) (all formations)	3.1 W/m/K
Composite thermal conductivity model (Moridis et al., 2008c)	$k_{\theta C} = k_{\theta RD} + (S_A^{1/2} + S_H^{1/2}) (k_{\theta RW} - k_{\theta RD}) + \phi S_l k_{\theta l}$
Capillary pressure model (vanGenuchten, 1980)	$P_{cap} = -P_0 \left[ (S^*)^{-1/\lambda} - 1 \right]^\lambda$ $S^* = \frac{(S_A - S_{irA})}{(S_{mxA} - S_{irA})}$
$S_{irA}$	1
$\lambda$ (White, 2008)	0.77437
$P_0$ (White, 2008)	$5 \times 10^3$ Pa
Relative permeability model (Moridis et al., 2008b)	$k_{rA} = (S_A^*)^n$ $k_{rG} = (S_G^*)^m$ $S_A^* = (S_A - S_{irA}) / (1 - S_{irA})$ $S_G^* = (S_G - S_{irG}) / (1 - S_{irA})$ EPM model
$n$ ; $m$ (from Anderson et al., 2008)	4.2; 2.5
$S_{irG}$	0.02
$S_{irA}$	0.20

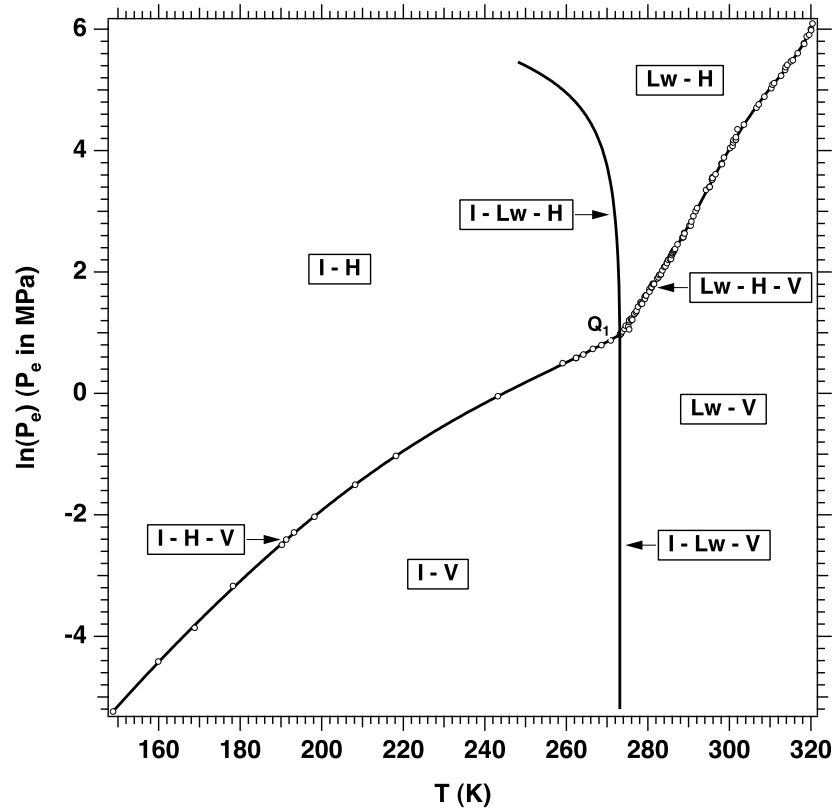


Figure 1. Pressure-temperature equilibrium relationship in the phase diagram of the water-CH<sub>4</sub>-hydrate system (Moridis, 2003), Lw: Liquid water; H: Hydrate; V: Vapor (gas phase); I: Ice; Q<sub>1</sub>: Quadruple point = I + Lw + H + V). The two arrows show the direction of increasing thermodynamic desirability of a deposit as a production target.

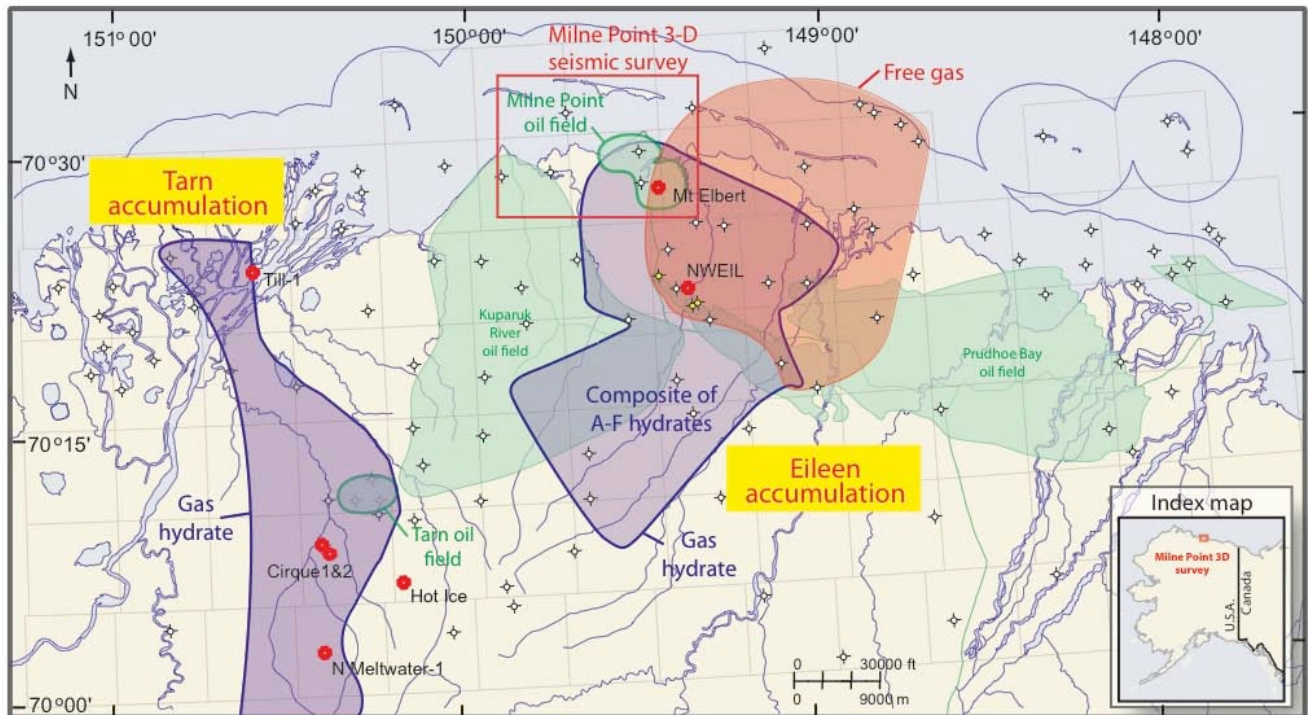


Figure 2 - Map of the Eileen and Tarn gas hydrate accumulations overlying portions of the Prudhoe Bay, Kuparuk River, and Milne Point oil fields (modified from Collett, 1993). The locations of the Northwest Eileen State-2 (NWEIL) and Mount Elbert gas hydrate research wells are shown, along with the outline of the Milne Point 3D seismic volume used to identify and map gas hydrate prospects.

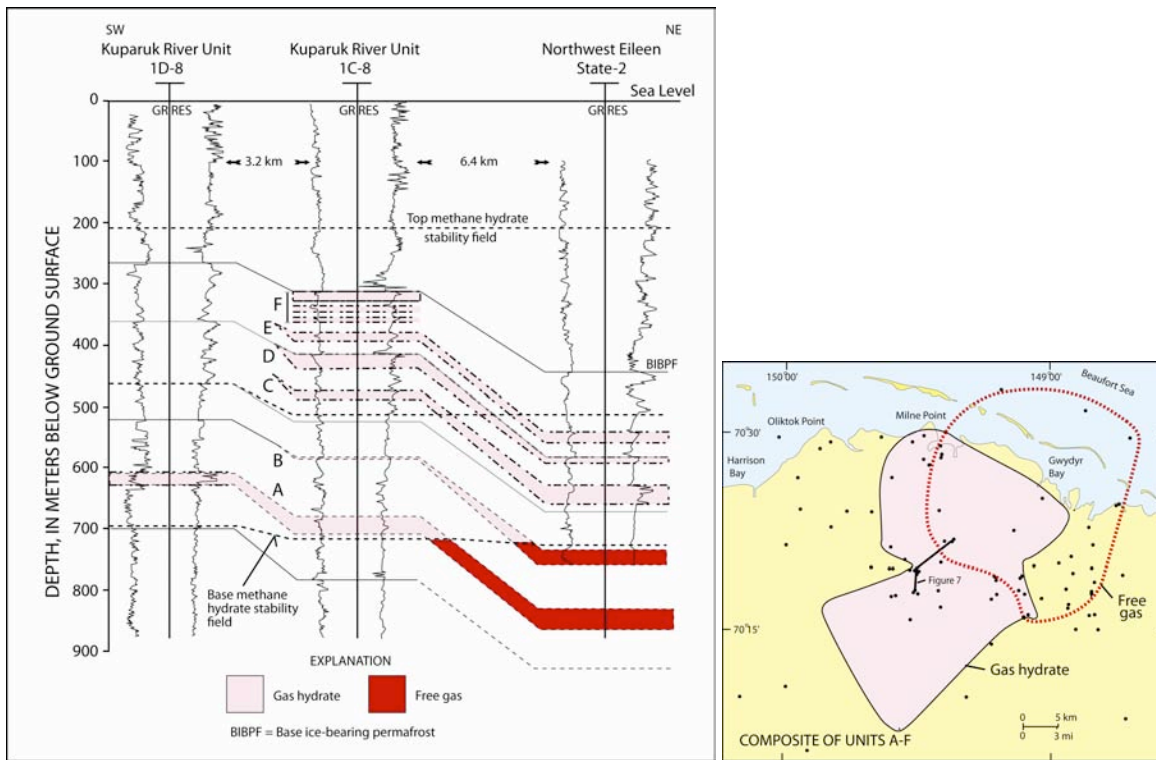


Figure 3. (a) Cross section showing the lateral and vertical extent of gas hydrates and underlying free-gas occurrences in the Prudhoe Bay-Kuparuk River area in northern Alaska. See Figure 3(b) for location of cross section. The gas-hydrate-bearing units are identified with the reference letters A through F (Collett, 1993), and their positions relative to the permafrost and to the base of the hydrate stability zone are shown; (b) Composite map of all six gas-hydrate/free-gas units (Units A-F) from the Prudhoe Bay-Kuparuk River area in northern Alaska (Collett, 1993).

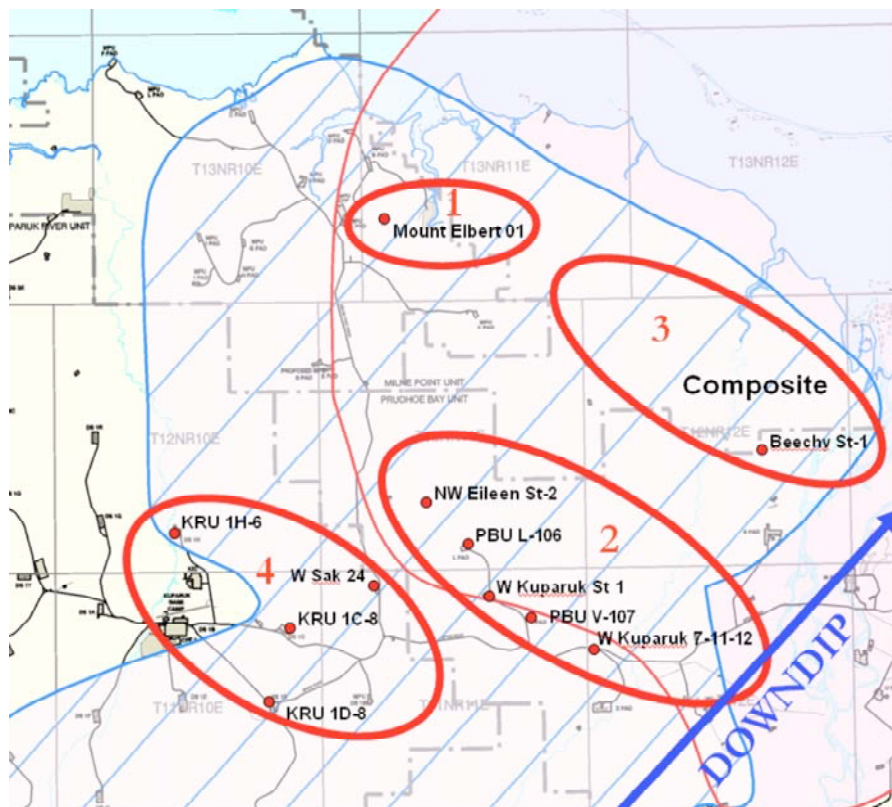


Figure 4: Map of composite lateral extent of Sagavanirktok gas hydrate bearing zones A, B, C, D, E, and F (blue with stripes) showing the relative locations of the Mount Elbert and PBU L-106 sites.

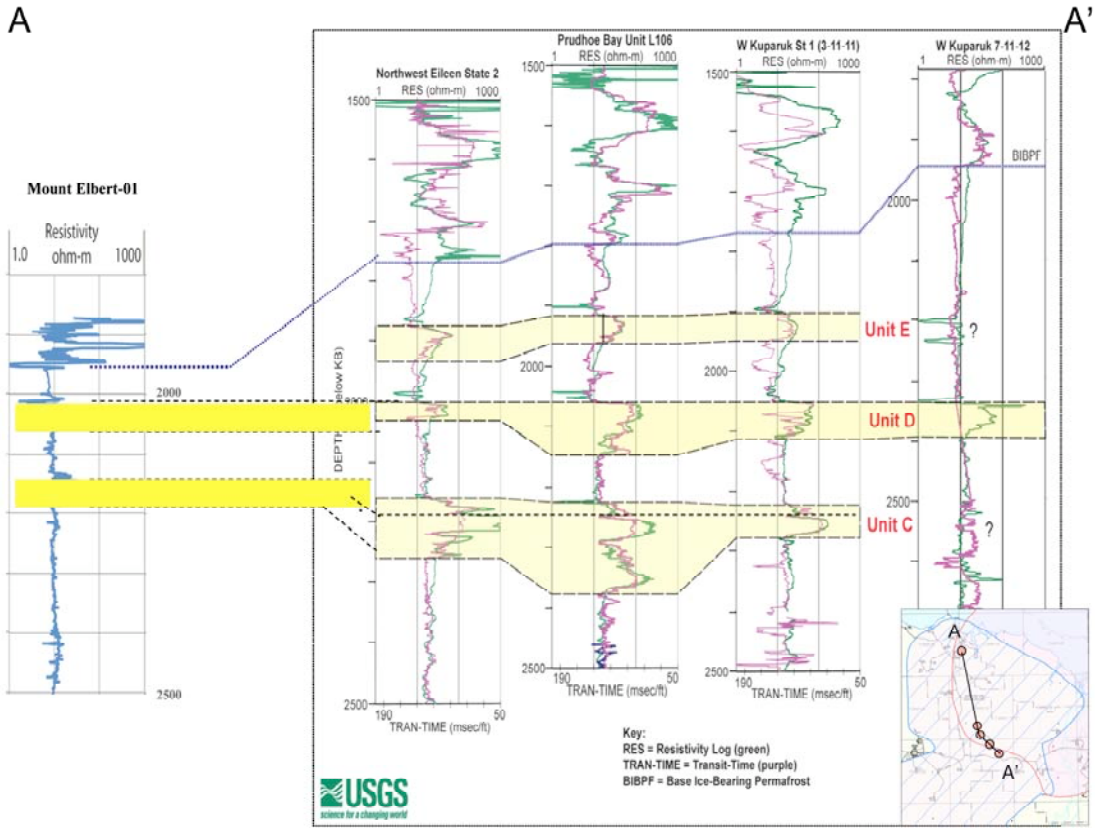


Figure 5: Cross section “downdip” from Mount Elbert across Area 2 (see Figure 4), through the PBU L-106 well.

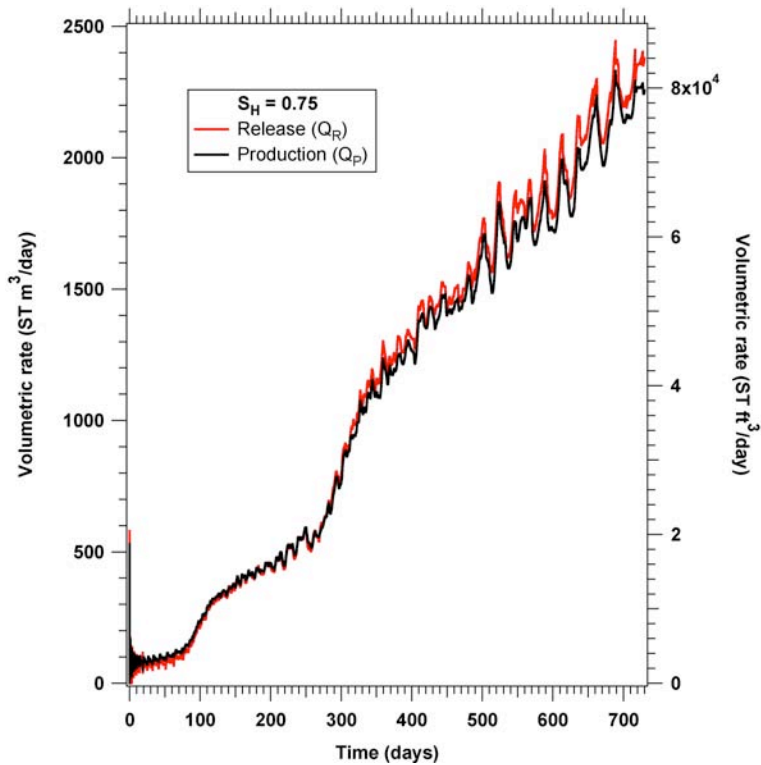


Figure 6 -  $Q_R$  and  $Q_P$  during a proposed long-term production test from the hydrate deposits in the C-Unit at the PBU L-106 site using depressurization-induced dissociation and a single vertical well: reference case ( $S_{H0} = 0.75$ ).

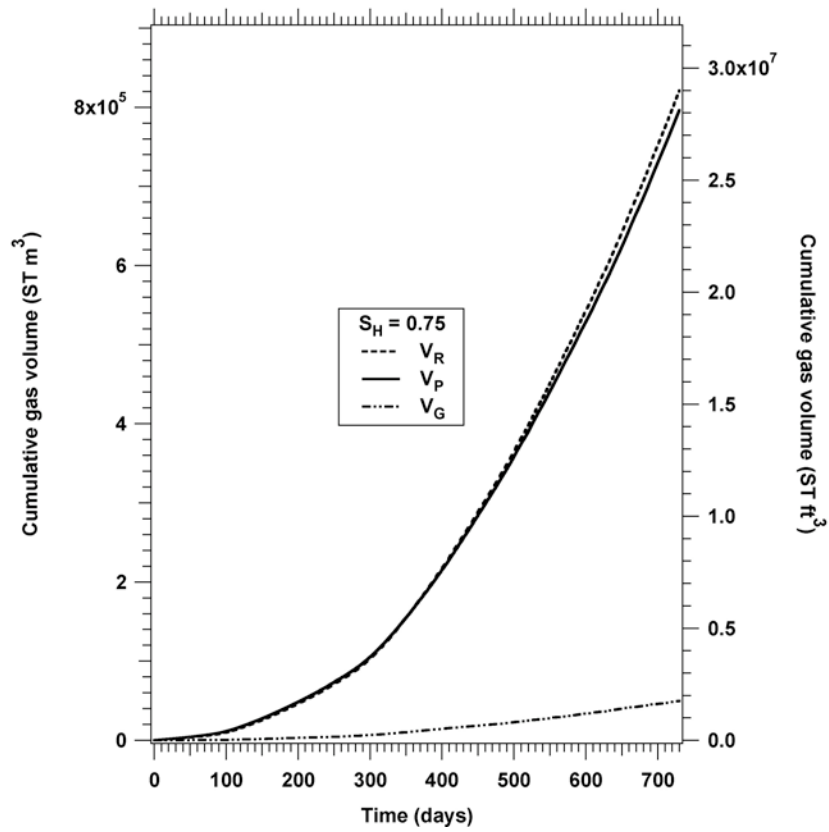


Figure 7 -  $V_R$ ,  $V_P$  and  $V_F$  during a proposed long-term production test from the hydrate deposits in the C-Unit at the PBU L-106 site using depressurization-induced dissociation and a single vertical well: reference case ( $S_{H0} = 0.75$ ).

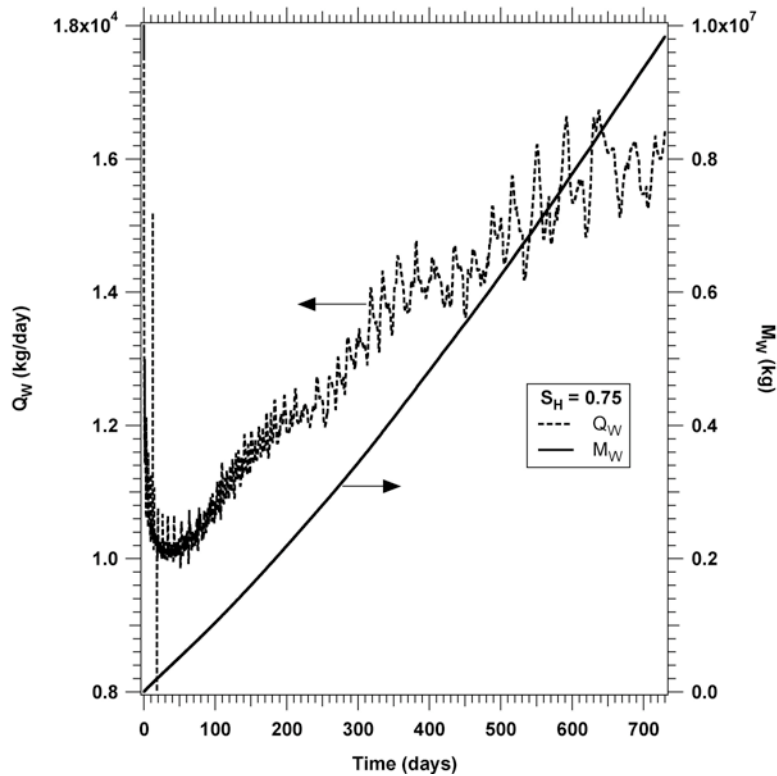


Figure 8 -  $Q_W$  and  $M_W$  during a proposed long-term production test from the hydrate deposits in C-Unit at the PBU L-106 site using depressurization-induced dissociation and a single vertical well: reference case ( $S_{H0} = 0.75$ ).

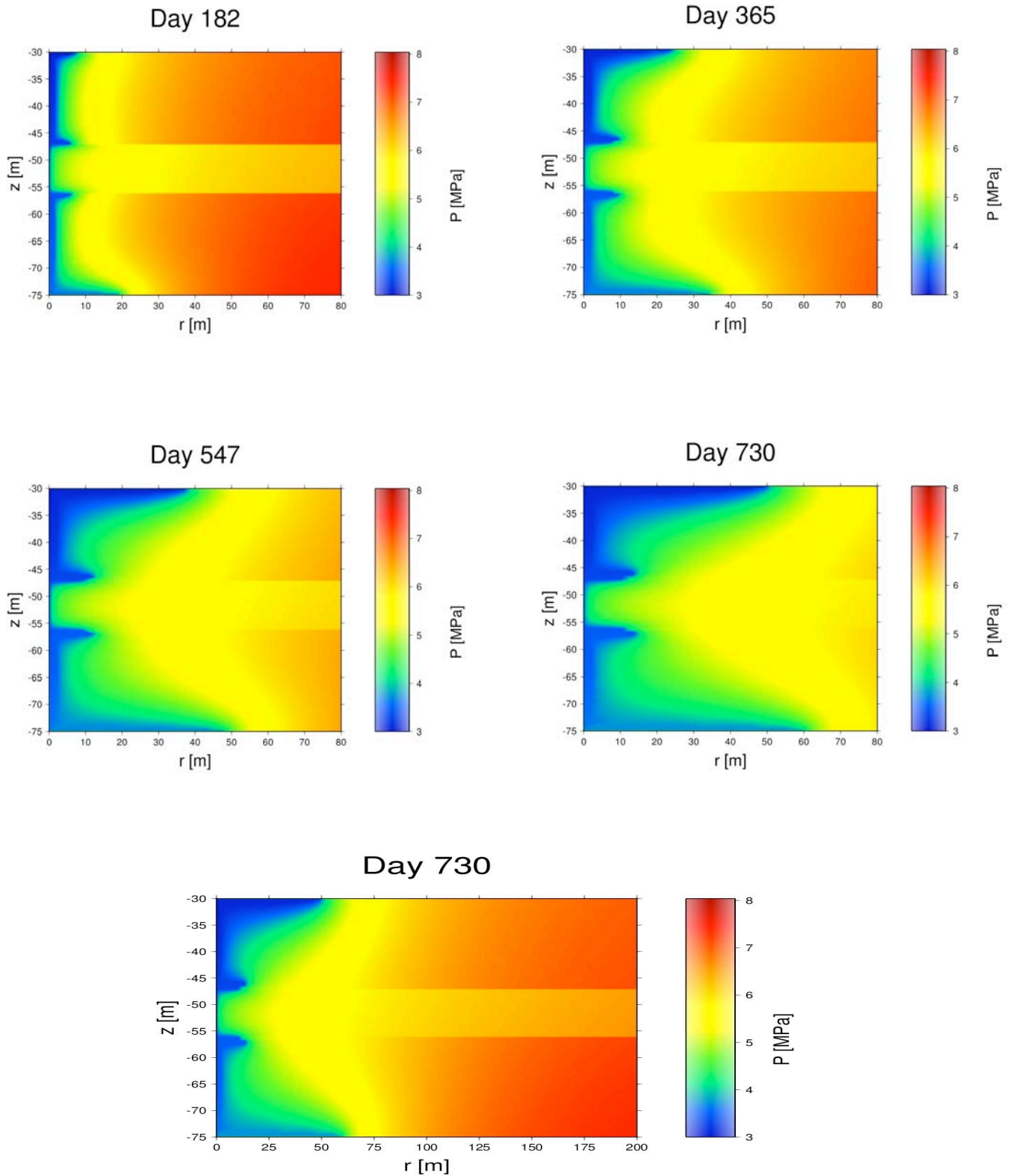


Figure 9 - Evolution of the  $P$ -distribution over time within  $r = 80$  m from the well during a depressurization-based long-term test of gas production from the C-Unit at the PBU L-106 site using a single vertical well ( $S_{H0} = 0.75$ ).

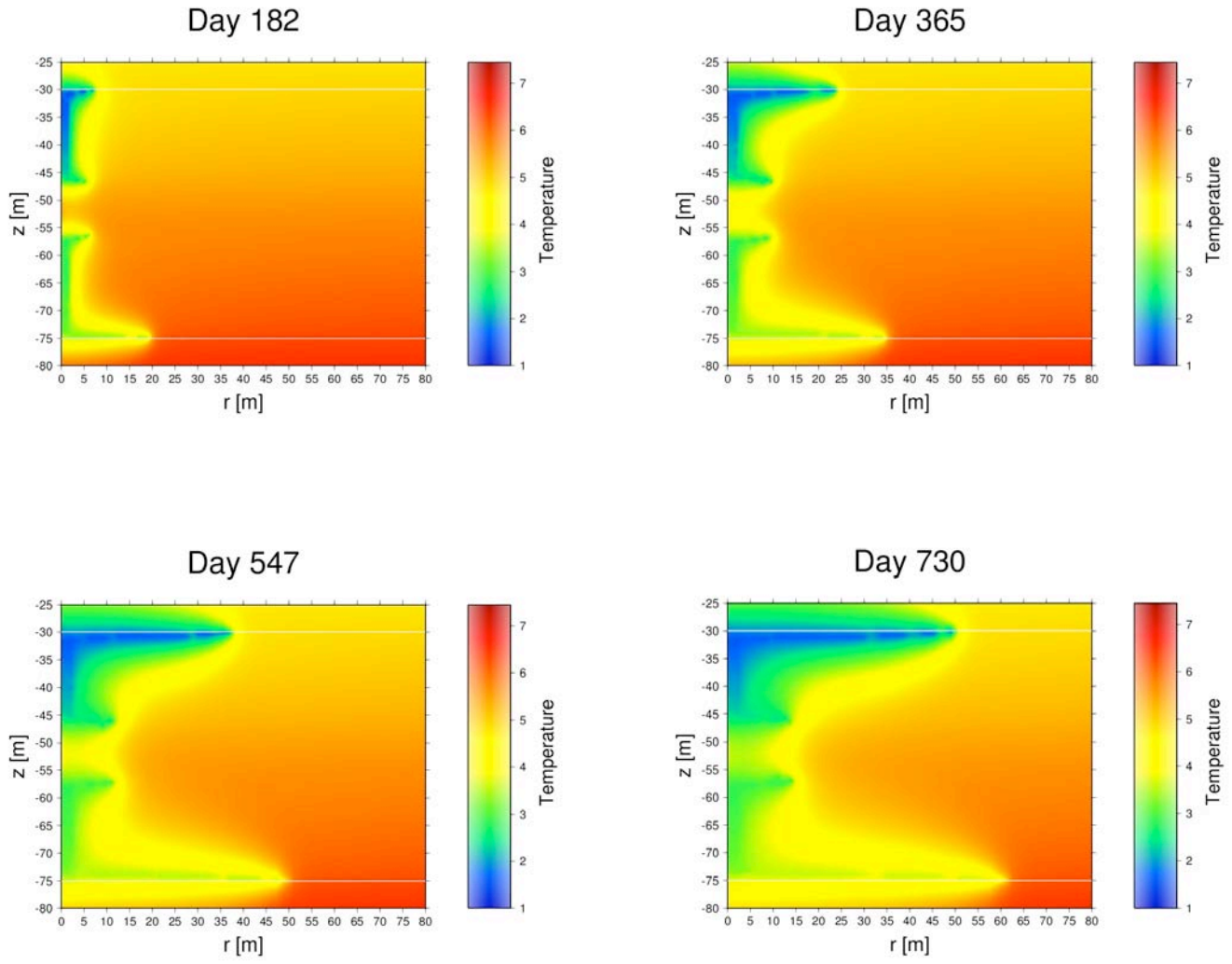


Figure 10 - Evolution of the  $T$ -distribution over time within  $r = 80$  m from the well during a depressurization-based long-term test of gas production from the C-Unit at the PBU L-106 site using a single vertical well ( $S_{H0} = 0.75$ ).

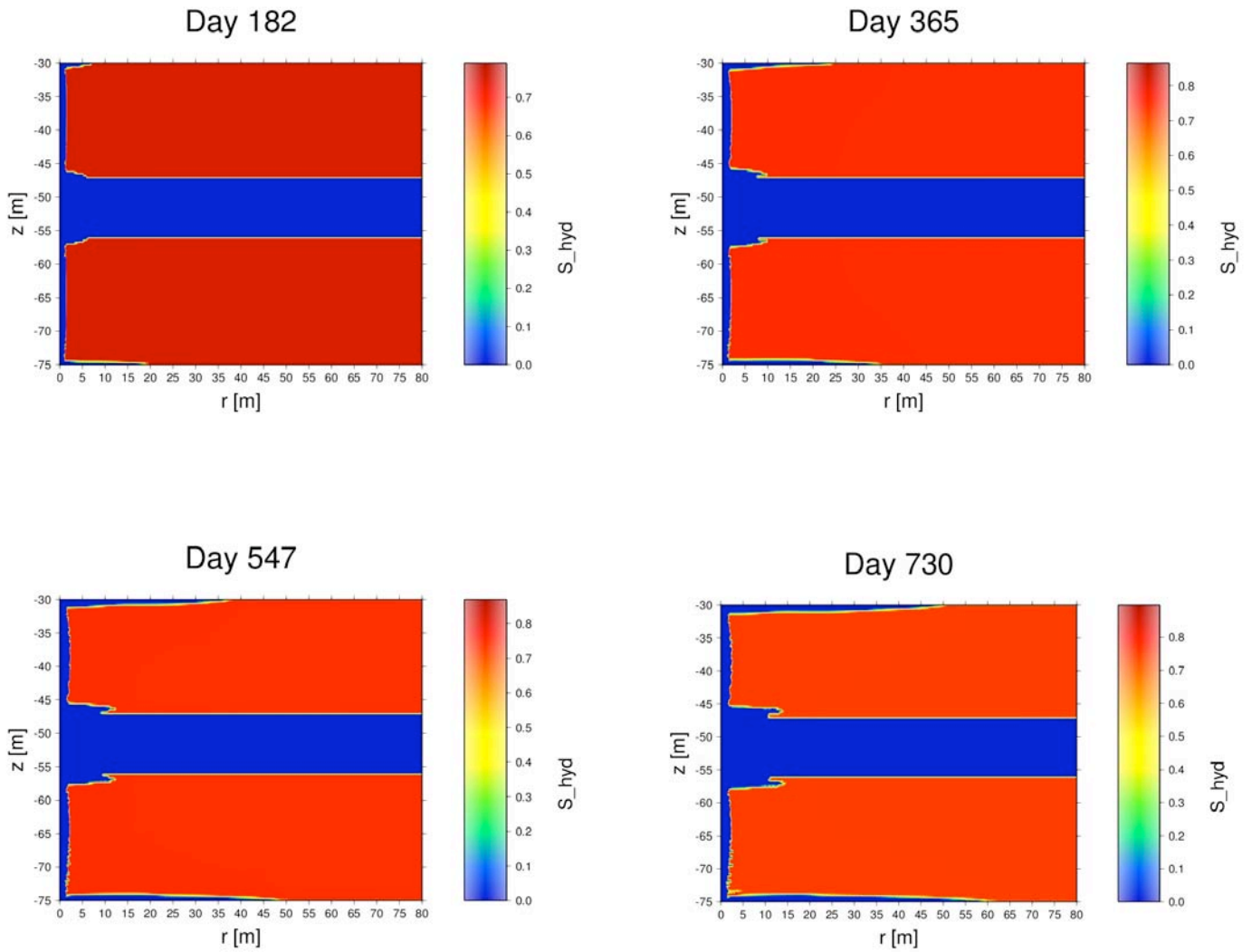


Figure 11 - Evolution of the  $S_r$ -distribution over time within  $r = 80$  m from the well during a depressurization-based long-term test of gas production from the C-Unit at the PBU L-106 site using a single vertical well ( $S_{H0} = 0.75$ ).

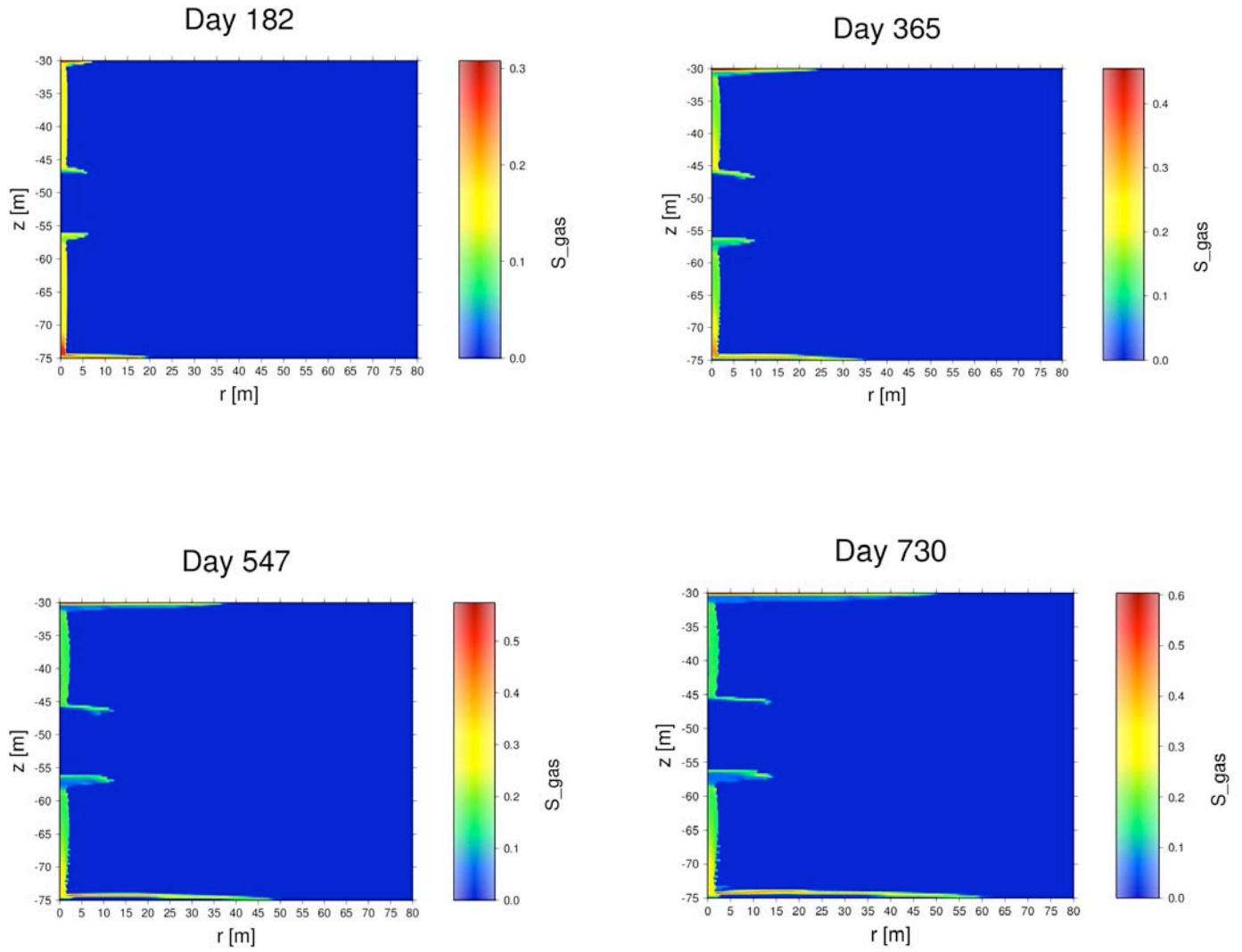


Figure 12 - Evolution of the  $S_g$ -distribution over time within  $r = 80$  m from the well during a depressurization-based long-term test of gas production from the C-Unit at the PBU L-106 site using a single vertical well ( $S_{H0} = 0.75$ ).

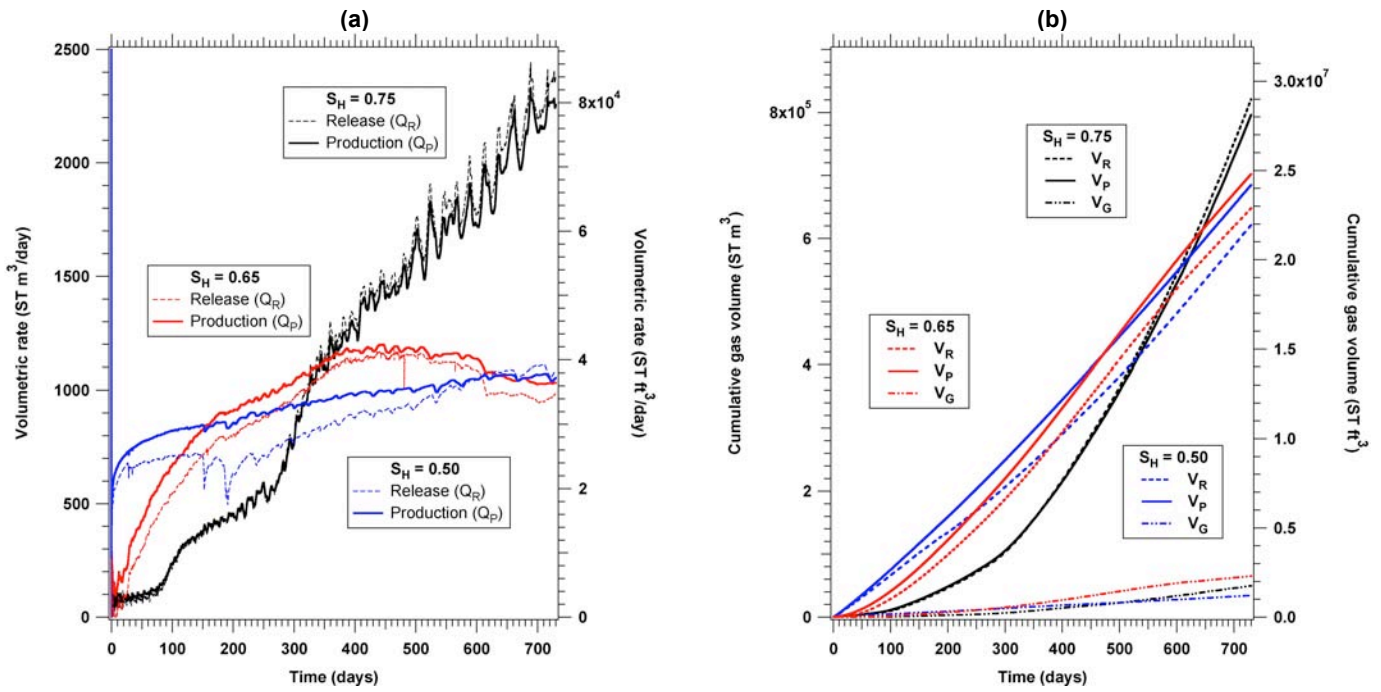


Figure 13 – Effect of  $S_H$  on gas production from the C-Unit at the PBU L-106 site using depressurization-induced dissociation and a single vertical well: (a)  $Q_R$  and  $Q_P$ , and (b)  $V_R$ ,  $V_P$  and  $V_F$ .

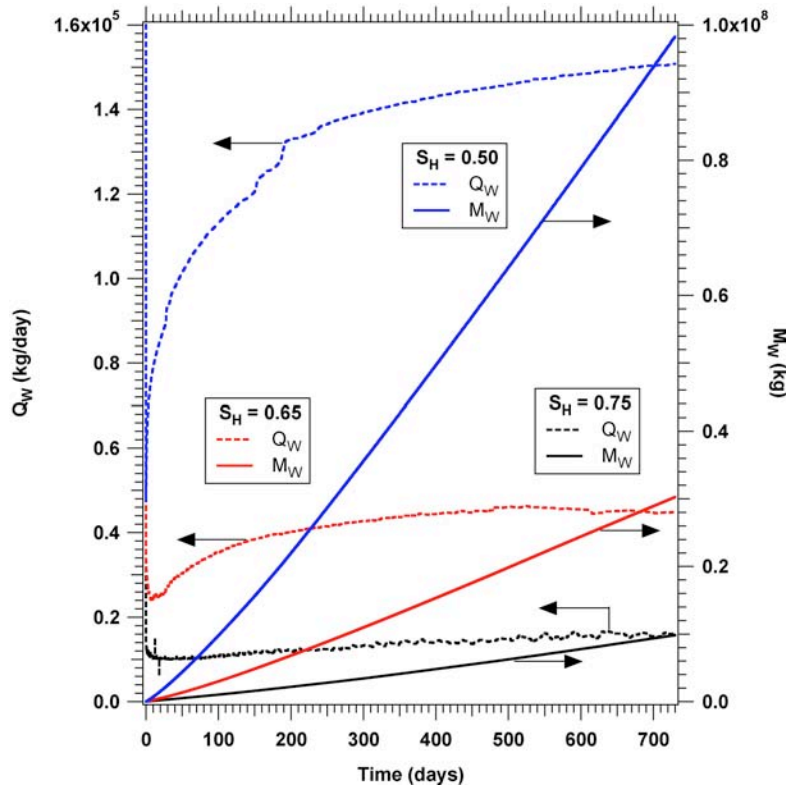


Figure 14 – Effect of  $S_H$  on water production ( $Q_W$  and  $M_W$ ) from the C-Unit at the PBU L-106 site during depressurization-based production from hydrates using a single vertical well.

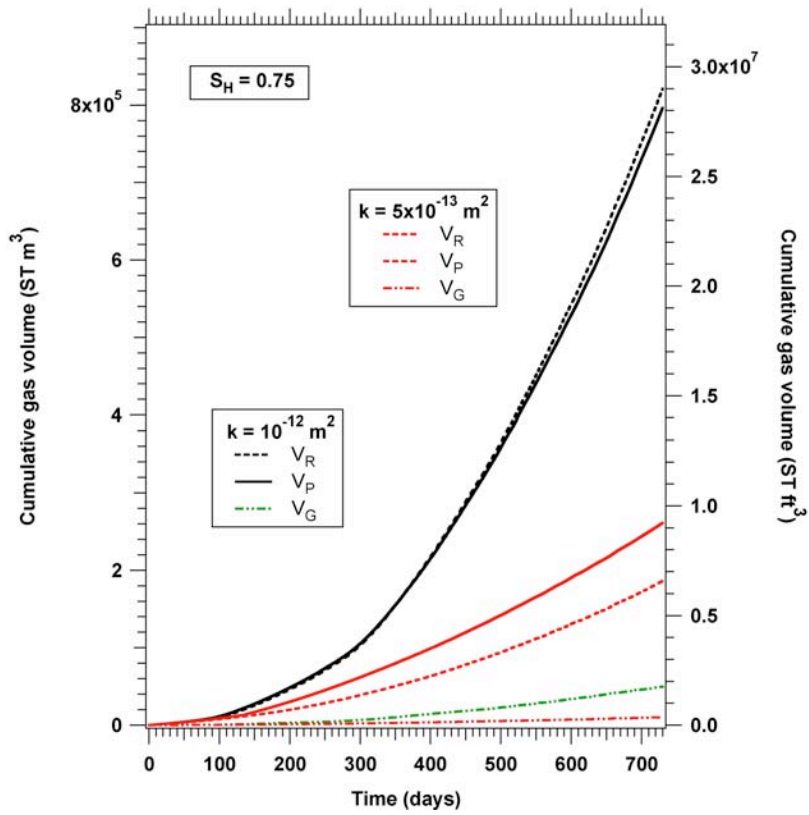


Figure 15 – Effect of intrinsic permeability  $k$  on gas production ( $V_R$ ,  $V_P$  and  $V_F$ ) from the C-Unit at the PBU L-106 site using depressurization-induced dissociation and a single vertical well ( $S_{H0} = 0.75$ ).

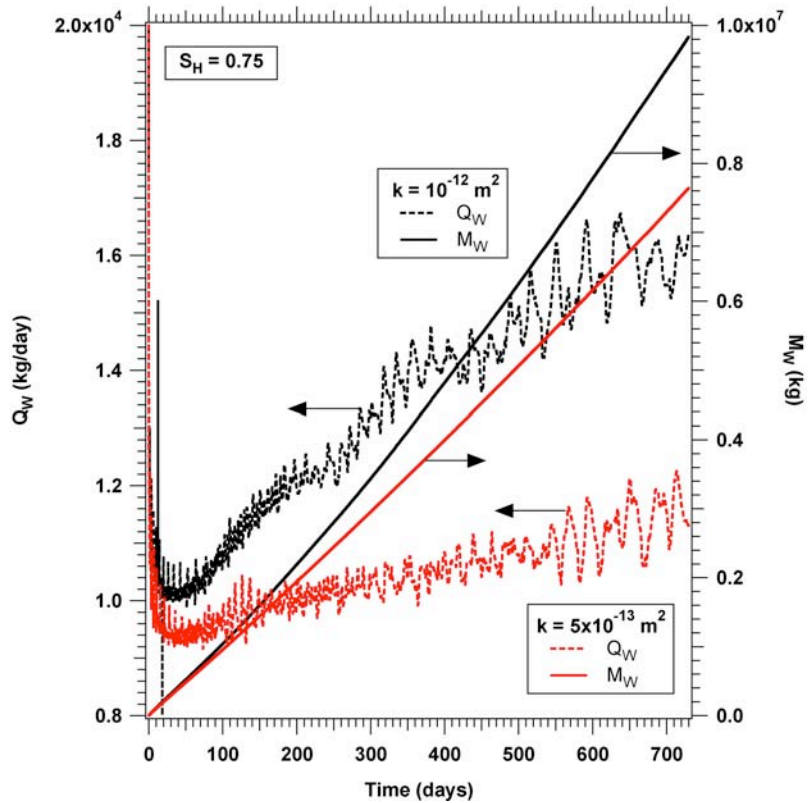


Figure 16 – Effect of intrinsic permeability  $k$  on water production ( $Q_W$  and  $M_W$ ) from the C-Unit at the PBU L-106 site during depressurization-based production from hydrates using a single vertical well ( $S_{H0} = 0.75$ ).

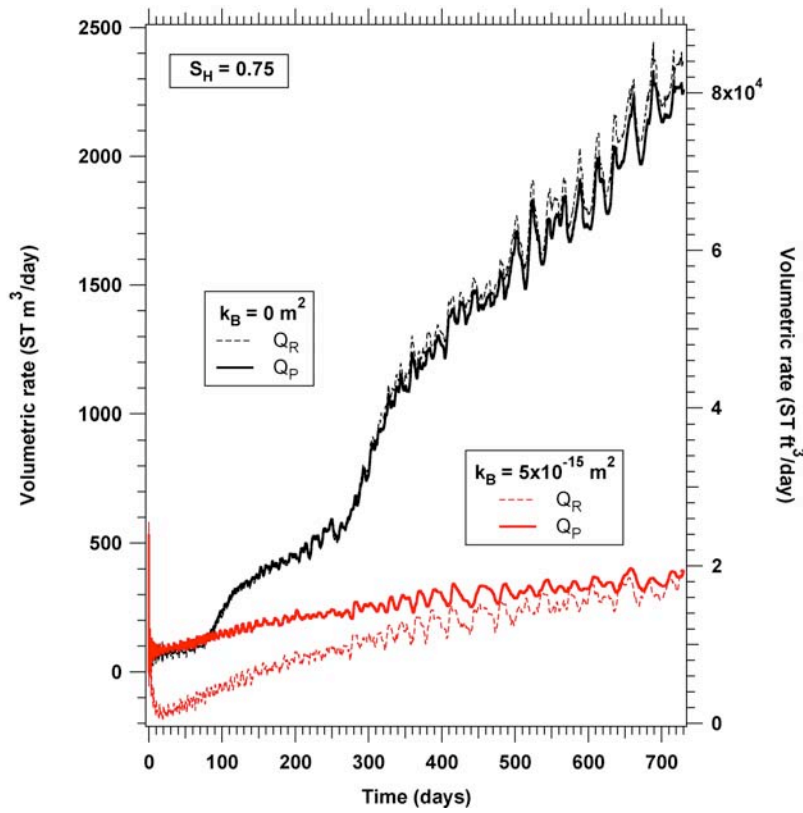


Figure 17 – Effect of the intrinsic permeability of the shale boundaries  $k_B$  on gas production ( $Q_R$  and  $Q_P$ ) from the C-Unit at the PBU L-106 site using depressurization-induced dissociation and a single vertical well ( $S_{H0} = 0.75$ ).

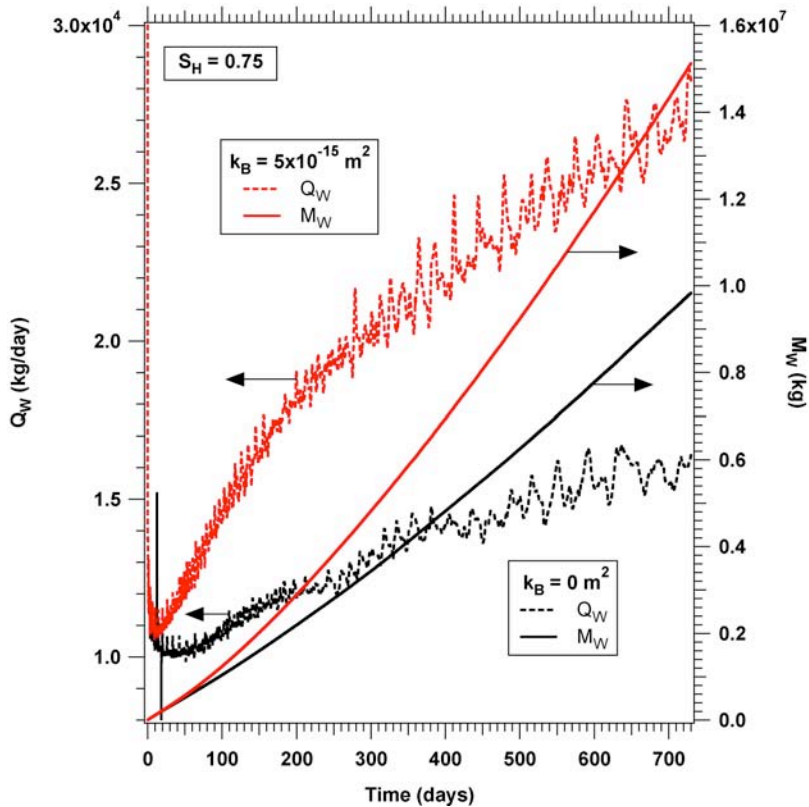


Figure 18 – Effect of intrinsic permeability  $k$  on water production ( $Q_W$  and  $M_W$ ) from the C-Unit at the PBU L-106 site during depressurization-based production from hydrates using a single vertical well ( $S_{H0} = 0.75$ ).

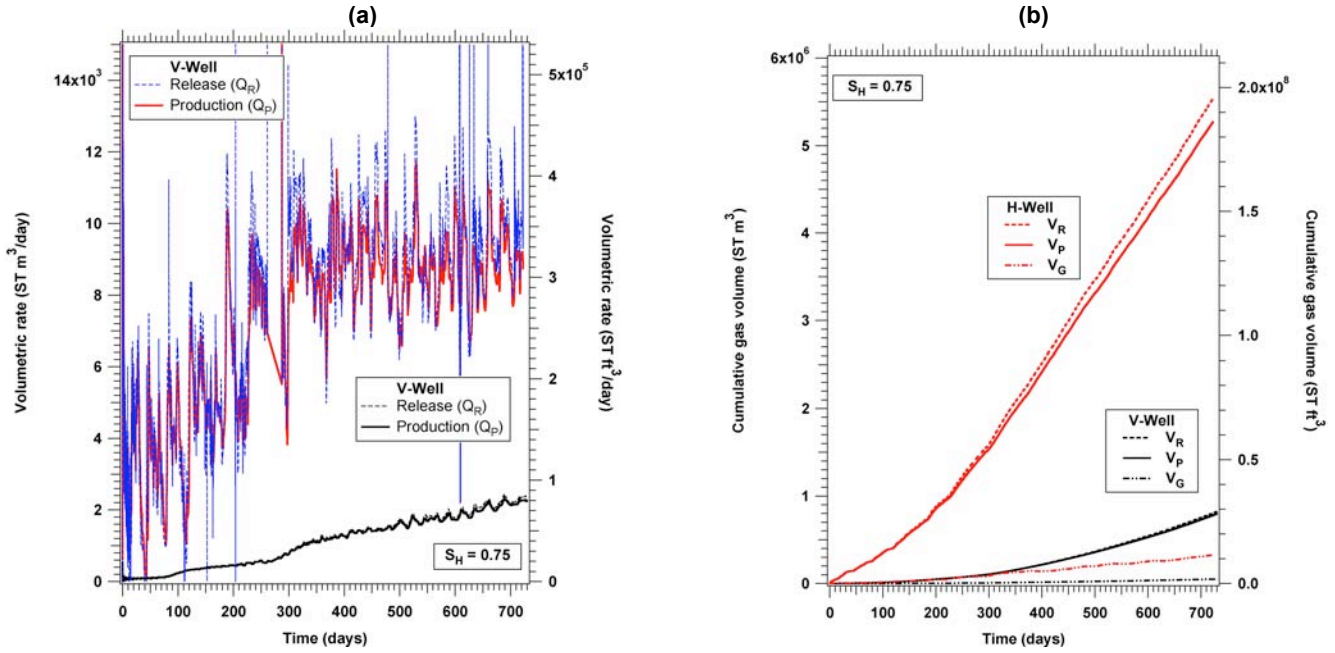


Figure 19 – (a)  $Q_R$  and  $Q_P$ , and (b)  $V_R$ ,  $V_P$  and  $V_F$  describing gas production from the C-Unit at the PBU L-106 site using depressurization-induced dissociation: horizontal vs. a single vertical well ( $S_{H0} = 0.75$ ).

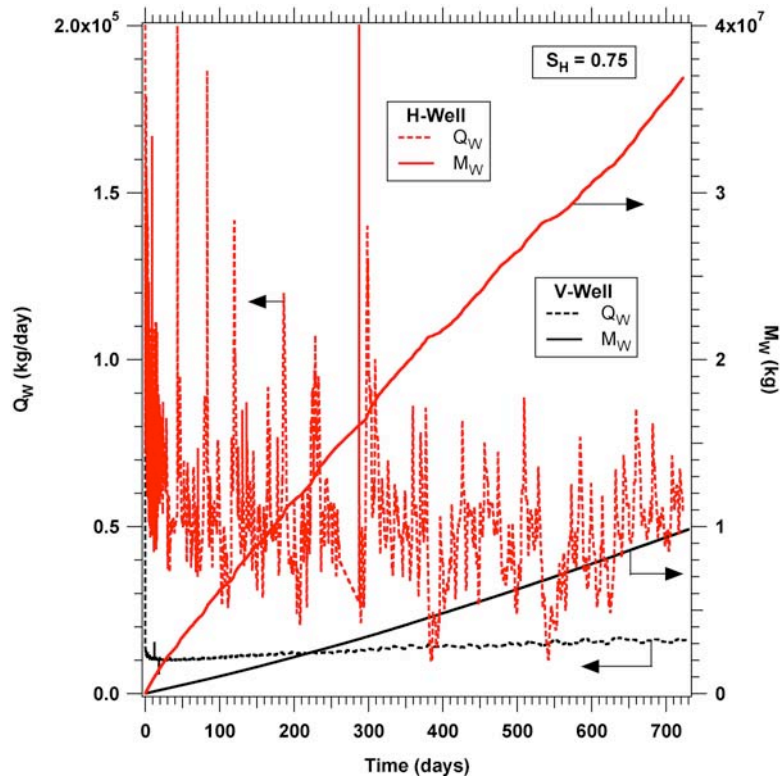


Figure 20 – Water production ( $Q_W$  and  $M_W$ ) from the C-Unit at the PBU L-106 site during depressurization-based production from hydrates: horizontal vs. a single vertical well ( $S_{H0} = 0.75$ ).

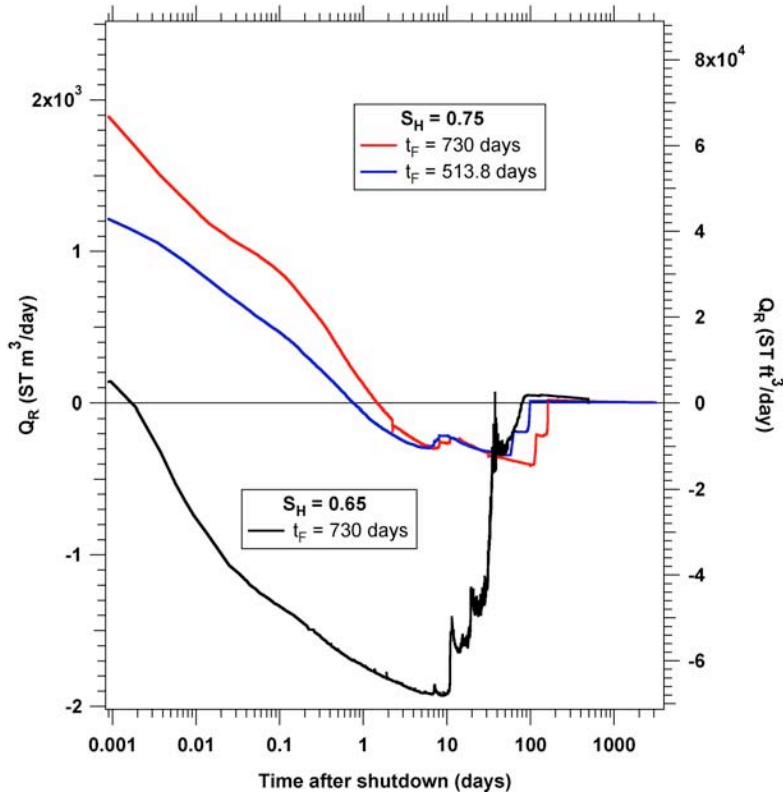


Figure 21 – Response of the C-Unit at the PBU L-106 site to the cessation of production (well shut-in) at a time  $t_F$ . ( $Q_W$  and  $M_W$ ) from the C-Unit at the PBU L-106 site during depressurization-based production from hydrates using a single vertical well ( $S_{H0} = 0.75$ ).

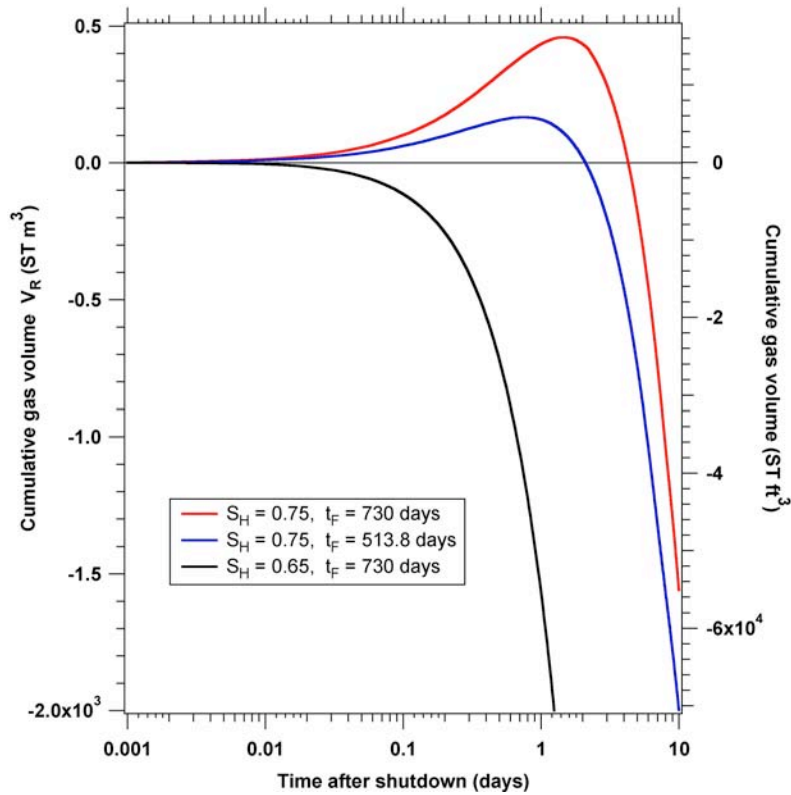


Figure 22 – Early response of the C-Unit at the PBU L-106 site to the cessation of production (well shut-in) at a time  $t_F$ . ( $Q_W$  and  $M_W$ ) from the C-Unit at the PBU L-106 site during depressurization-based production from hydrates using a single vertical well ( $S_{H0} = 0.75$ ).

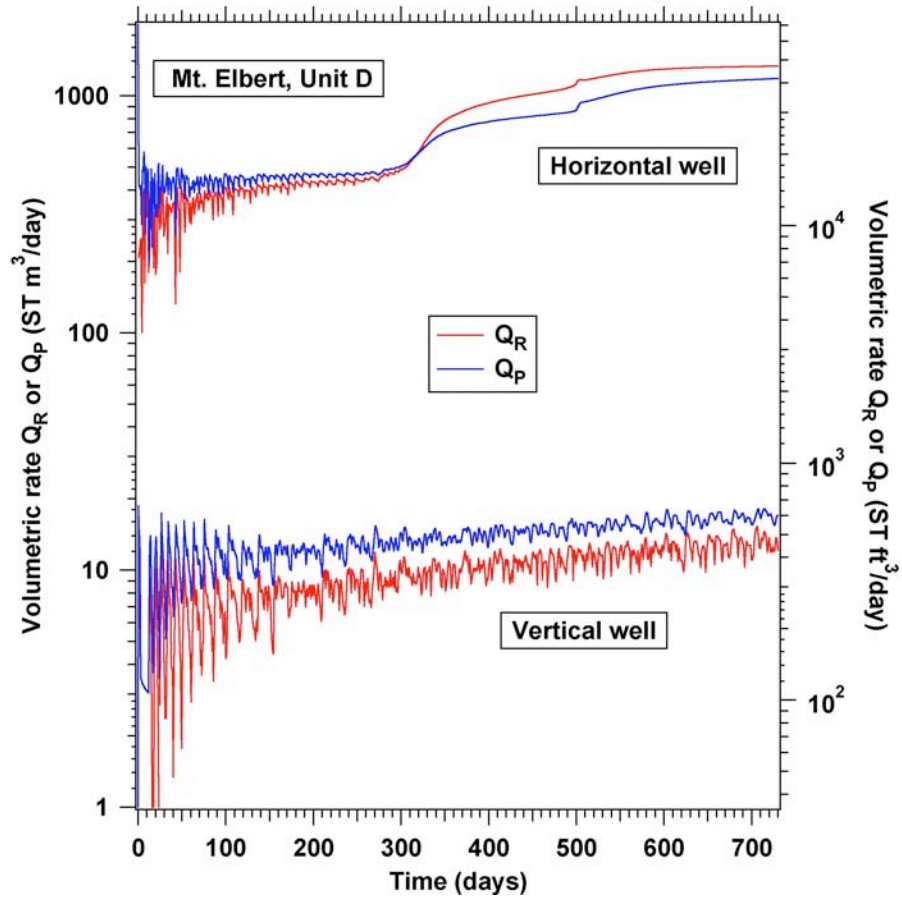


Figure 23 -  $Q_R$  and  $Q_P$  during a proposed long-term production test from the hydrate deposit in the D-Unit at the Mount Elbert site using depressurization-induced dissociation - horizontal well and a single vertical well (Moridis et al., 2010b).

## DISCLAIMER

This document was prepared as an account of work sponsored by the United States Government. While this document is believed to contain correct information, neither the United States Government nor any agency thereof, nor The Regents of the University of California, nor any of their employees, makes any warranty, express or implied, or assumes any legal responsibility for the accuracy, completeness, or usefulness of any information, apparatus, product, or process disclosed, or represents that its use would not infringe privately owned rights. Reference herein to any specific commercial product, process, or service by its trade name, trademark, manufacturer, or otherwise, does not necessarily constitute or imply its endorsement, recommendation, or favoring by the United States Government or any agency thereof, or The Regents of the University of California. The views and opinions of authors expressed herein do not necessarily state or reflect those of the United States Government or any agency thereof or The Regents of the University of California.

Ernest Orlando Lawrence Berkeley National Laboratory is an equal opportunity employer.